

Industrial Chemistry Publication Series

Teknillisen kemian julkaisusarja

Espoo 2004

No. 17

KINETIC MODELING OF LIQUID-PHASE HYDROGENATION REACTIONS

Mikko Lylykangas

Dissertation for the degree of Doctor of Science in Technology to be presented with due permission of the Department of Chemical Technology for public examination and debate in Auditorium Ke 2 (Komppa Auditorium) at Helsinki University of Technology (Espoo, Finland) on the 13th of February, 2004, at 12 o'clock noon.

Helsinki University of Technology
Department of Chemical Technology
Laboratory of Industrial Chemistry

Teknillinen korkeakoulu
Kemian tekniikan osasto
Teknillisen kemian laboratorio

Distribution:

Helsinki University of Technology

Laboratory of Industrial Chemistry

P. O. Box 6100

FIN-02015 HUT

Tel. +358-9-4511

Fax. +358-9-451 2622

E-Mail: arja.tuohino@hut.fi

© Mikko Lylykangas

ISBN 951-22-6912-0 (print), 951-22-6913-9 (pdf, available at <http://lib.hut.fi/Diss/>)

ISSN 1235-6840

Otamedia Oy

Espoo 2004

PREFACE

The work described in this thesis was carried out in the Laboratory of Industrial Chemistry, Helsinki University of Technology, between June 1999 and August 2003. Funding from the National Technology Agency of Finland (Tekes) and Fortum Oil and Gas Oy is gratefully acknowledged. Additionally, the Academy of Finland is thanked for its support through the Graduate School in Chemical Engineering (GSCE).

I am most grateful to Professor Outi Krause and Dr. Petri Rautanen for their invaluable help throughout the preparation of this thesis. Furthermore, I gratefully acknowledge my co-author Dr. Reetta Karinen for the isomerization equilibrium determinations and Mr. Tuomo Keskitalo for his help with the reactor simulations. Mr. Antti Hasanen, Ms. Eeva-Maija Ryymin, and Mr. Kim Tarpila have been of great help in obtaining the kinetic data. Also, many thanks to my colleagues and the laboratory staff, who have made the atmosphere at work enjoyable.

Finally, my warmest thanks to Noora.

Espoo, January 2004

Mikko Lylykangas

ABSTRACT

Kinetic models are an essential part of modern computer simulation based process design. The goal of the work presented here was to develop models for two types of industrially important hydrogenation reactions, namely the hydrogenation of mono- and diaromatic compounds and the hydrogenation of isooctenes. The studied reactions are important in the production of new, environmentally friendly fuels. Saturation of aromatics is needed to limit the undesired particle emissions in the exhaust gases of diesel engines, and isooctane could be used to replace methyl-*tert*-butyl ether (MTBE) in gasoline as an octane rating increasing component.

The hydrogenation of aromatics was studied on a commercial Ni/Al₂O₃ catalyst using three model compounds: toluene, 1,2,3,4-tetrahydronaphthalene (tetralin), and naphthalene. The results showed that the first ring of the diaromatic compound (naphthalene) is considerably more reactive than the second, whereas the hydrogenation rate of the monoaromatic compounds (toluene and tetralin) is only slightly affected by the structure of the substituent. In addition, an inhibition effect induced by competitive adsorption was observed in the hydrogenation of multicomponent mixtures. The most reactive compound adsorbs most strongly on the catalyst and inhibits the other reactions. Hydrogenation was assumed to proceed by a mechanism of stepwise addition of dissociatively adsorbed hydrogen. Langmuir–Hinshelwood type rate equations were able to describe the reaction kinetics successfully, including the inhibition effect. The estimated adsorption parameters in the mixtures increased with reactivity ($K_{\text{toluene}} = 1.0 \times 10^{-3} \text{ m}^3/\text{mol}$, $K_{\text{tetralin}} = 4.4 \times 10^{-3} \text{ m}^3/\text{mol}$, $K_{\text{naphthalene}} = 7.8 \times 10^{-3} \text{ m}^3/\text{mol}$). Additionally, the estimated activation energies were in the physically meaningful range of 26–59 kJ/mol.

The hydrogenation of the isooctenes 2,4,4-trimethyl-1-pentene (TMP-1) and 2,4,4-trimethyl-2-pentene (TMP-2) to “isooctane” (IO; 2,2,4-trimethylpentane) was examined on commercial Ni/Al₂O₃, Co/SiO₂, and Pt/Al₂O₃ catalysts. Qualitatively, the hydrogenation proceeded in the same way on the different catalysts in that TMP-1 (terminal double bond) was more reactive than TMP-2 (internal double bond), isooctane was the sole product, and double bond isomerization did not play an important role under the conditions used. Kinetic models were formulated on the basis of the two-step Horiuti–Polanyi mechanism, assuming rate limitation by the

first hydrogen insertion. The difference in the activities (Ni > Co > Pt) of the three catalysts was concluded to be due to the number of active sites because turnover frequencies (TOFs) were of the same order of magnitude. However, in some features, Pt was found to deviate from Ni and Co in the hydrogenation of TMP-1 and TMP-2. Activation energies were higher ($E_{app,TMP-1} = 49$ kJ/mol on Pt and 34–35 kJ/mol on Ni and Co; $E_{app,TMP-2} = 65$ kJ/mol on Pt and 43–49 kJ/mol on Ni and Co) and hydrogen adsorption equilibrium constants were larger by two orders of magnitude ($K_H = 38 \times 10^{-4}$ m³/mol on Pt, 0.16×10^{-4} m³/mol on Ni, and 0.30×10^{-4} m³/mol on Co). In addition, catalyst deactivation through the formation of carbonaceous deposits was considerably faster on Pt.

The kinetic equations developed in this work are applicable as such in reactor design because mass transfer, hydrogen solubility, and solvent effect were taken into account in the parameter optimization. In the hydrogenation of aromatics, valuable information was obtained on how to describe hydrogenation reactions in multicomponent mixtures, such as real diesel fractions. The results from the hydrogenation of TMP-1 and TMP-2 provide information that can be applied to the selection of an optimal catalyst material as well as in the design and optimization of industrial-scale reactors.

LIST OF PUBLICATIONS

This thesis is derived from the following publications, which are referred to in the text by the corresponding Roman numerals:

- I Rautanen, P. A.; Lylykangas, M. S.; Aittamaa, J. R.; Krause, A. O. I. Liquid Phase Hydrogenation of Naphthalene on Ni/Al₂O₃. *Stud. Surf. Sci. Catal.* **133** (2001) 309–316.
- II Lylykangas, M. S.; Rautanen, P. A.; Krause, A. O. I. Liquid-Phase Hydrogenation Kinetics of Multicomponent Aromatic Mixtures on Ni/Al₂O₃. *Ind. Eng. Chem. Res.* **41** (2002) 5632–5639.
- III Karinen, R. S.; Lylykangas, M. S.; Krause, A. O. I. Reaction Equilibrium in the Isomerization of 2,4,4-Trimethyl Pentenes. *Ind. Eng. Chem. Res.* **40** (2001) 1011–1015.
- IV Lylykangas, M. S.; Rautanen, P. A.; Krause, A. O. I. Liquid-Phase Hydrogenation Kinetics of Isooctenes on Ni/Al₂O₃. *AIChE J.* **49** (2003) 1508–1515.
- V Lylykangas, M. S.; Rautanen, P. A.; Krause, A. O. I. Liquid-Phase Hydrogenation Kinetics of Isooctenes on Co/SiO₂. *Appl. Catal. A: Gen.* (2004), in press.
- VI Lylykangas, M. S.; Rautanen, P. A.; Krause, A. O. I. Hydrogenation and Deactivation Kinetics in the Liquid-Phase Hydrogenation of Isooctenes on Pt/Al₂O₃. *Ind. Eng. Chem. Res.* (2004), accepted for publication.

Contribution of the author to the publications:

- I Mikko Lylykangas participated in the research planning and experimental work and contributed to the writing of the manuscript.
- II, IV Mikko Lylykangas participated in the research planning, performed the experiments, interpreted the results together with the co-authors and wrote the manuscript.
- III Mikko Lylykangas contributed to the interpretation of the results and to the writing of the manuscript.
- V, VI Mikko Lylykangas made the research plan, performed the experiments, interpreted the results, carried out the kinetic modeling and wrote the manuscript.

CONTENTS

PREFACE.....	1
ABSTRACT.....	2
LIST OF PUBLICATIONS	4
CONTENTS.....	6
1. INTRODUCTION	7
2. EXPERIMENTAL.....	11
2.1. Catalysts.....	11
2.2. Test Reactor	13
2.3. Mass-Transfer Experiments	13
2.4. Kinetic Experiments.....	14
3. KINETIC MODELING	15
3.1. Models for Mass and Heat Transfer.....	15
3.2. Reactor Model.....	17
3.3. Minimization of the Objective Function.....	18
4. HYDROGENATION OF AROMATIC COMPOUNDS	19
4.1. Qualitative Hydrogenation Results	19
4.2. Catalyst Deactivation	21
4.3. Hydrogenation Kinetics	22
4.4. Validation of the Kinetic Models.....	25
5. HYDROGENATION OF ISOCTENES	27
5.1. Thermodynamic Equilibrium between Isooctenes.....	27
5.2. Qualitative Hydrogenation Results	27
5.3. Catalyst Deactivation	28
5.4. Hydrogenation Kinetics	30
5.5. Usability of Ni, Co, and Pt Catalysts on the Industrial Scale	35
6. COMMON FEATURES IN HYDROGENATION.....	37
7. CONCLUSIONS.....	39
8. LIST OF ABBREVIATIONS AND SYMBOLS	40
9. REFERENCES	42

APPENDICES: PUBLICATIONS I–VI

1. INTRODUCTION

The increased attention paid to catalytic hydrogenation in the oil refining industry is due in part to legislation regarding the maximum contents of sulfur, aromatic compounds, and alkenes in traffic fuels.^{1,2} Aromatics in diesel increase the particle emissions in exhaust gases³ and they have the further effect of lowering the fuel quality.² Alkenes in gasoline are undesired in larger amounts because of higher NO_x and CO formation and the higher reactivity of evaporative emissions in comparison to their saturated counterparts.⁴ The specifications for diesel and gasoline quality that will come into effect in 2005 in the EU are shown in Table 1.

Table 1. The EU specifications for diesel (left) and gasoline (right).⁵

Diesel	EU 2005	Gasoline	EU 2005
Density [kg/m ³]	< 845	Aromatics [vol %]	< 35
Cetane no. [-]	> 51	Alkenes [vol %]	< 18
Distill. T ₉₅ [°C]	< 360	Benzene [vol %]	< 1.0
PAH [w %]	< 11	Oxygen [vol %]	< 2.7
Sulfur [w %]	< 0.005	Sulfur [w %]	< 0.005

Key objectives in the development of new hydrogenation processes include the development of more active catalysts as well as accurate kinetic models that are based on reaction mechanisms. When carried out on the industrial scale, the reactions related with this work are performed in the liquid phase, in order to avoid excessive energy consumption during the vaporization of the reactants. Using the liquid phase complicates kinetic studies and makes most of the in-situ techniques for mechanistic determinations impossible. Higher concentrations and equilibrium limitation in the hydrogen solubility in the liquid phase may, however, substantially change the hydrogenation and deactivation rates. With this in mind, it appeared prudent to perform the experiments under conditions as close to the industrial operating conditions as possible, that is in the liquid phase at moderate temperatures and elevated pressures.

Despite the large extent to which the hydrogenation of aromatic compounds has been studied no consensus exists about the reaction mechanism. In principle, two

types of mechanisms have been proposed. The first suggests that the hydrogenation of the aromatic ring proceeds through sequential additions of adsorbed hydrogen atoms.⁶⁻⁹ The other involves addition of molecular hydrogen from the bulk gas or liquid to the aromatic ring and subsequent complex formation. This complex retains its aromatic nature through the second hydrogenation step, after which it isomerizes to the corresponding cyclohexene. The cyclic alkene is then hydrogenated to the fully saturated product.¹⁰⁻¹² The nature of hydrogen that is active in hydrogenation varies thus from dissociated H atoms to the H₂ that undergoes an Eley-Rideal type of addition reaction.

The first part of the present study concerned the hydrogenation of mono- and diaromatic compounds to model the dearomatization of diesel (Papers I and II). Kinetic models were developed that can be used in the design and optimization of industrial-scale reactors. Rate equations (generalized Langmuir-Hinshelwood type) were based on the assumption of a stepwise addition mechanism of adsorbed hydrogen atoms. Kinetic parameters were optimized from the data obtained on a commercial Ni/Al₂O₃ catalyst. Traditionally, sulfided NiMo, CoMo, and NiW hydrotreating catalysts have been used, which act both as desulfurization and dearomatization catalysts. However, in order to meet the tightening limitations for diesel (Table 1), high temperature, high hydrogen pressure, and low space velocities are required.¹³ The increased temperature leads to thermodynamic equilibrium limitation especially in the hydrogenation of aromatic compounds,^{13,14} and high hydrogen pressure and low space velocities are not always economically viable. Therefore, a two-stage process has been developed, in which heteroatom compounds are removed in the first stage with a sulfided hydrotreating catalyst and aromatic compounds are hydrogenated in the second stage with a supported noble metal or nickel catalyst.¹³⁻¹⁶ Nickel has the advantage of low price and reaction temperatures compared to noble metal catalysts, but it is less tolerant to feed impurities, sulfur compounds in particular. The forthcoming legislation requires more efficient removal of sulfur compounds in the hydrotreating stage, and therefore nickel seems as a favorable hydrogenation catalyst in the processing of future diesel fractions.

Three compounds toluene, tetralin, and naphthalene were used as models for the mono- and diaromatic compounds in diesel. The model compounds were hydrogenated both separately and as mixtures because the feed to an industrial-scale

hydrogenation reactor contains several types of mono- and polyaromatic compounds. In such multicomponent mixtures, competitive adsorption is expected to affect the hydrogenation rates.^{17,18} Furthermore, the applicability of kinetic equations based on single-compound experiments was examined using these equations to simulate the reaction kinetics in mixtures (Paper II).

In contrast to aromatics, there is little dispute in the literature about the mechanism of alkene double bond hydrogenation on supported metal catalysts. A two-step addition mechanism of chemisorbed H atoms, as first proposed by Horiuti and Polanyi in the 1930s¹⁹ is generally accepted.^{20,21} Recently, the focus has been on IR-spectroscopic measurements to determine the different adsorption modes of alkenes on the catalyst surface.²²⁻²⁵ These studies have shown that at least three different forms are present: π -bonded, di- σ -bonded, and ethylidyne species. It appears that the hydrogenation rate of the alkene is practically uncorrelated with the surface concentration of the both ethylidyne (hydrogen-deficient) and di- σ -bonded (dissociatively adsorbed) species.²⁶⁻²⁹ This has led to the conclusion that the hydrogenation path includes π -bonded alkene attached to a single metal atom on both nickel and noble metal catalysts,³⁰⁻³² which agrees well with the description of double-bond hydrogenation as a structure-insensitive reaction.³³⁻³⁵

In the second part of this thesis, the hydrogenation of isooctenes, 2,4,4-trimethyl-1-pentene (TMP-1) and 2,4,4-trimethyl-2-pentene (TMP-2), to the isooctane, 2,2,4-trimethylpentane (IO), was studied (Papers III–VI). Isooctane, due to its high octane number and low vapor pressure, is an attractive choice to replace MTBE in gasoline.³⁶⁻³⁸ This has led to the introduction of process configurations for isooctane production through dimerization of isobutene and hydrogenation of isooctene (dimerization product).^{39,40} Isooctene has almost equally good fuel properties as isooctane, but because of the limitations imposed upon the alkene content in gasoline (Table 1), it must be hydrogenated. The kinetic models developed for this thesis for the hydrogenation were based on the Horiuti–Polanyi mechanism. The role of double-bond isomerization in the course of hydrogenation reactions was also established. For this, the thermodynamic equilibrium of TMP-1 and TMP-2 was determined prior to the hydrogenation experiments (Paper III). Hydrogenation was then performed using non-equilibrium feeds of TMP-1 and TMP-2. Different commercial catalysts were tested: Ni/Al₂O₃ (Paper IV), Co/SiO₂ (Paper V), and Pt/Al₂O₃ (Paper VI). The

comparative study of these catalysts can help to choose the most suitable catalyst material to be used on the industrial scale.

2. EXPERIMENTAL

2.1. Catalysts

Three different commercial catalysts were applied to the hydrogenation: Ni/Al₂O₃ (16.6 wt %) in Papers I–II and IV, Co/SiO₂ (21.5 wt %) in Paper V, and Pt/Al₂O₃ (0.3 wt %) in Paper VI. The number of active sites per gram of each catalyst was measured using hydrogen chemisorption. Additionally, the BET-surface area and pore volume of the Pt/Al₂O₃ catalyst was measured using nitrogen physisorption. These measurements were carried out with a static chemisorption/physisorption equipment (Omnisorp 100CX).

In the chemisorption measurements, a sample of catalyst was evacuated and heated (10 °C/min) in a quartz glass U-tube to 150 °C, after which it was purged with helium for 30 min. Thereafter, the sample was again evacuated and heated (10 °C/min) to the reduction temperature of 400 °C. This reduction temperature was experimentally determined to result in the highest possible active surface area. The catalyst was reduced in flowing hydrogen for a period of 4 h (2 h for Ni/Al₂O₃⁴¹), then evacuated at 450 °C for 4 h (2 h for Ni/Al₂O₃⁴¹) to remove any traces hydrogen. The catalyst was then cooled under vacuum to the chemisorption temperature (30 °C for Ni and Pt, 100 °C for Co), at which the isotherm of total adsorption was determined up to 3.3×10^4 Pa. The measurement of total adsorption was followed by an evacuation period of 60 min to remove reversibly adsorbed hydrogen and to allow the measurement of the reversible adsorption isotherm. The irreversible chemisorption was obtained by subtracting the amount of reversibly adsorbed hydrogen from the total hydrogen uptake.

Nitrogen physisorption measurements for the platinum catalyst were performed at the temperature of liquid nitrogen. Before taking the measurement, the sample was outgassed at 90 °C for two hours and then at 350 °C until the pressure in the sample holder was 4×10^{-4} Pa. Thereafter, the sample was cooled down to the temperature of liquid nitrogen at which both the adsorption and desorption isotherms were measured.

On Ni/Al₂O₃, the number of active sites was determined from the amount of irreversibly adsorbed hydrogen.⁴¹ The results corresponded to a specific surface area of 108 m²/g_{Ni} and a number of active sites of 2.7×10^{20} atoms/g_{cat}. The reason for choosing the higher chemisorption temperature on Co/SiO₂ was that hydrogen

chemisorption on cobalt is reported to be an activated process.⁴²⁻⁴⁴ Indeed, measurements at various adsorption temperatures revealed that the amount of adsorbed hydrogen was higher at 100 °C than at 30 °C on Co, in contrast to Ni and Pt catalysts on which the adsorption isotherms did not vary markedly across the same temperature range. Furthermore, the active surface area on Co was calculated differently from Ni and Pt catalysts. The calculations for Co were based on the total chemisorption because the amount of irreversibly adsorbed hydrogen was dependent upon the duration of the evacuation period between the total and reversible isotherm measurements. The specific surface area and the number of active sites on Co were $11 \text{ m}^2/\text{g}_{\text{Co}}$ and $3.5 \times 10^{19} \text{ atoms}/\text{g}_{\text{cat}}$, respectively. On Pt/Al₂O₃ the metal surface area was determined similarly to the Ni catalyst. According to the measurements, the specific surface area was $214 \text{ m}^2/\text{g}_{\text{Pt}}$, which corresponds to a number of active sites of $8.8 \times 10^{18} \text{ atoms}/\text{g}_{\text{cat}}$. A summary of the chemisorption methods and results is presented in Table 2.

Table 2. Hydrogen chemisorption results for the catalysts.

Catalyst	Adsorption T [°C]	Adsorption type	Area [m ² /g _{met}]	No. of sites [atoms/g _{cat}]
Ni/Al ₂ O ₃	30	irreversible	105	2.7×10^{20}
Co/SiO ₂	100	total	11	3.5×10^{19}
Pt/Al ₂ O ₃	30	irreversible	214	8.8×10^{18}

In order to model internal mass-transfer effects, knowledge of the structure of the catalyst particles is essential (see section 3.1). The quantities needed for the catalyst particles are the density (ρ_p), porosity (ϵ_p), and tortuosity (τ_p). For the nickel catalyst, the density was measured ($\rho_p = 2200 \text{ kg}/\text{m}^3$) and typical values from the literature were used for the porosity and tortuosity ($\epsilon_p = 0.50$, $\tau_p = 4.0$).⁴⁵ In the study with the cobalt catalyst, the density was measured ($\rho_p = 2100 \text{ kg}/\text{m}^3$) and a literature value was used for the tortuosity ($\tau_p = 3.8$).⁴⁵ The porosity value ($\epsilon_p = 0.60$) was based on the density and mean pore volume $0.30 \text{ cm}^3/\text{g}$ given by the catalyst manufacturer. In the study with the platinum catalyst, the density and tortuosity values ($\rho_p = 1250 \text{ kg}/\text{m}^3$, $\tau_p = 4.0$) were obtained in the same manner as for the Ni and Co catalysts. The

porosity value was calculated from the results of the nitrogen physisorption measurements. These results showed that the BET-area of the platinum catalyst was 192 m²/g and the total pore volume was 0.54 cm³/g, which corresponds, together with the density of the particle, to a porosity, ϵ_p , of 0.68. Values of the physical properties of the catalysts are presented in Table 3.

Table 3. Physical properties of the catalysts.

Catalyst	ρ_p [kg/m ³]	τ_p [-]	ϵ_p [-]
Ni/Al ₂ O ₃	2200 ^a	4.0 ^b	0.50 ^b
Co/SiO ₂	2100 ^a	3.8 ^b	0.60 ^c
Pt/Al ₂ O ₃	1250 ^a	4.0 ^b	0.68 ^a

^a Measured value. ^b Average value. ^c Value given by the catalyst manufacturer.

2.2. Test Reactor

Hydrogenation experiments were performed in a continuous stirred laboratory-scale three-phase reactor equipped with a fixed catalyst basket and a magnetic stirrer. The gas (258 cm³_{NTP}/min in Papers I and II, 70 cm³_{NTP}/min in Papers IV–VI) and liquid (50 g/h) feeds were regulated using mass flow controllers. The reaction pressure was maintained at the desired level by regulating the gas outlet stream, which was separated from the liquid product in a high-pressure separation unit. The liquid product samples were analyzed on-line using a gas chromatograph with a fused silica capillary column and an FI detector.

2.3. Mass-Transfer Experiments

The gas–liquid and liquid–solid mass-transfer resistances were determined experimentally by varying the catalyst loading in the reactor. An estimate of the external mass-transfer limitations could be made by plotting the reciprocal of the conversion rate (mol/h) as a function of the reciprocal of catalyst mass and extrapolating the catalyst mass to an infinitely high value (intercept with the 1/ m_{cat} axis). The mass-transfer rates thereby obtained were considerably higher than the maximum reaction rates observed in the kinetic experiments. Thus, it was concluded that external mass transfer did not have an effect on the observed rates in the hydrogenation experiments.

Experiments with various particle sizes and high values of the Weisz–Prater criterion ($\Phi \gg 1$) showed, however, that internal mass-transfer limitations could not be avoided with the available experimental setup. The size of the screen opening in the catalyst basket meant that only particles above 0.5 mm in diameter could be used. Therefore, in the optimization of kinetic parameters, a model for the diffusion resistance inside the catalyst particles had to be included in the reactor model.

2.4. Kinetic Experiments

Each experiment was carried out with fresh catalyst that had first been dried at 110 °C in N₂. Prior to starting the liquid feed, the catalyst was reduced in situ at 400 °C for two hours with mixing in flowing hydrogen. Experiments in the continuously operating reactor were typically divided into periods of 4–5 h with different reaction conditions (temperature, pressure, and feed concentrations). In addition, a standard period with reference conditions was included at the beginning and end of the experiment to monitor the catalyst activity. This arrangement enabled collection of extensive data sets and elimination of the effect of catalyst deactivation on observed hydrogenation rates.

In the hydrogenation of aromatic compounds (Papers I and II), the pressure range was 20–40 bar, and temperatures of 85–160 °C (Paper I) and 80–140 °C (Paper II) were used. The total content of aromatic compounds varied between 1 and 36 mol % in n-decane solvent. In the hydrogenation of isooctenes the temperature range was 35–95 °C for the Ni and Co catalysts (Papers IV and V) and 80–140 °C for Pt (Paper VI). With each catalyst, the pressure ranged from 10 to 40 bar, and the feed contained 5–15 mol % isooctenes with varying ratios of TMP-1 and TMP-2 in cyclohexane solvent.

3. KINETIC MODELING

3.1. Models for Mass and Heat Transfer

The mass-transfer rate between the gas and liquid phases was described using the two-film theory:

$$N_{GL,i}a_{GL} = \frac{c_{G,i} - K_{GL,i}c_{L,i}}{\frac{K_{GL,i}}{\kappa_L a_{GL}} + \frac{1}{\kappa_G a_{GL}}} \quad (1)$$

Since experiments with various catalyst loadings had shown that the external mass transfer did not limit the rates of the reactions, high values were assigned for the mass-transfer coefficients in the gas and liquid films ($\kappa_G a_{GL} = 1.0 \times 10^4 \text{ s}^{-1}$ and $\kappa_L a_{GL} = 1.0 \times 10^2 \text{ s}^{-1}$). The equilibrium constants at the phase interface ($K_{GL,i}$) were evaluated using the Soave–Redlich–Kwong (SRK) equation of state in Papers I and II and the Peng–Robinson (PR) equation of state in Papers IV–VI. Both have been experimentally proven to be accurate methods for the calculation of vapor–liquid equilibrium between hydrogen and hydrocarbons.^{46–48} The reason for choosing the PR instead of the SRK equation of state in Papers IV–VI was that it is reported to produce a slightly better fit for mixtures of hydrogen and alkanes with a carbon number less than 20.⁴⁷

Diffusion inside the porous catalyst particles was described using the effective diffusion coefficients, $D_{\text{eff},i}$, which account for the mass-transfer restriction due to porous matter in accordance with

$$D_{\text{eff},i} = D_i \frac{\varepsilon_p}{\tau_p} \quad (2)$$

where D_i is the molecular diffusion coefficient, and ε_p and τ_p stand for the porosity and tortuosity inside of the particles, respectively. Molecular diffusion coefficients were estimated by the Wilke–Chang method,⁴⁹ and the values of ε_p and τ_p for the different catalysts were obtained by the methods described in section 2.1 (see Table 3). The mass-transfer rate between the liquid phase and the porous catalyst (observed reaction rates, $N_{LS,i}a_{LS}$) was obtained from the solution of the mole balance for the catalyst particles:

$$\frac{\partial c_i}{\partial t} = \frac{D_{\text{eff},i}}{\varepsilon_p r_p^2} \left[\frac{\partial^2 c_i}{\partial \lambda^2} + \frac{(B-1)}{\lambda} \frac{\partial c_i}{\partial \lambda} \right] + r_i \frac{\rho_p}{\varepsilon_p} \quad (3)$$

where λ stands for the dimensionless position inside the catalyst particles ($0 \leq \lambda \leq 1$) and r_p and ρ_p for the radius and density of the catalyst particles, respectively (see section 2.1). Parameter B is the shape factor of the catalyst particles, which is defined by

$$B = \frac{A_p}{V_p} r_p \quad (4)$$

where A_p and V_p stand for the outer surface area and volume of the particles, respectively. Crushed and sieved fractions of the Ni/Al₂O₃ and Co/SiO₂ catalysts were used, and therefore B had a value of 3 in Papers I–II and IV–V (spherical geometry). In Paper VI, strong deactivation on Pt/Al₂O₃ (see section 5.3) forced the use of industrial-size particles, which were long, cylindrical in shape and had a B parameter value of 2. The partial differential equation 3 was solved by discretizing it with respect to the position inside the particle (λ) using a five-point central difference formula. The mass-transfer rates at the liquid–solid interface (apparent rates), $N_{LS,i}a_{LS}$, were then calculated by summing up the rates in each discretization interval.

The gas and liquid bulk phases were assumed to be isothermal because the temperature of the stirred reaction vessel was controlled using external heating and cooling (± 0.5 °C). Furthermore, the maximum temperature difference inside the 0.5 mm Ni/Al₂O₃ and Co/SiO₂ catalyst particles according to

$$(\Delta T)_{\max} = \frac{\sum_i [c_i (-\Delta H_{R,i}) D_{\text{eff},i}]}{k_t} \quad (5)$$

was less than 0.3 °C. Therefore, the heat transfer in the catalyst could be ignored in the kinetic models in Papers I–II and IV–V. However, in Paper VI, because the industrial particle size (diameter 1.2 mm, length 5.1 mm) was used, isothermal particles could not be assumed. For this reason, the dynamic energy balance described by equation 6 was used to describe the temperature profile inside the catalyst particles:

$$\frac{\partial T}{\partial t} = \frac{k_t}{\rho_p c_p r_p^2} \left(\frac{\partial^2 T}{\partial \lambda^2} + \frac{1}{\lambda} \frac{\partial T}{\partial \lambda} \right) + \sum_i r_i \frac{(-\Delta H_{R,i})}{c_p} \quad (6)$$

In equation 6, the values of -113 kJ/mol and -117 kJ/mol were used for the heats of reaction (ΔH_R) in the hydrogenation of TMP-1 and TMP-2, respectively (Paper III).

For the heat conductivity (k_t) and specific heat capacity (c_p) of the catalyst particles, the values of $0.13 \text{ W/(m K)}^{50,51}$ and $0.85 \text{ J/(g K)}^{52}$ were assumed.

3.2. Reactor Model

The continuous stirred tank reactor was modeled with dynamic mole balances for the gas and liquid phases (Figure 1):

$$\frac{dn_i^G}{dt} = F_{in,i}^G - V_R N_{GL,i} a_{GL} - F_{out,i}^G \quad (7)$$

and

$$\frac{dn_i^L}{dt} = F_{in,i}^L + V_R N_{GL,i} a_{GL} + V_R N_{LS,i} a_{LS} - F_{out,i}^L \quad (8)$$

where the mass-transfer terms, $N_{GL,i} a_{GL}$ and $N_{LS,i} a_{LS}$, were calculated using the equations presented in section 3.1.

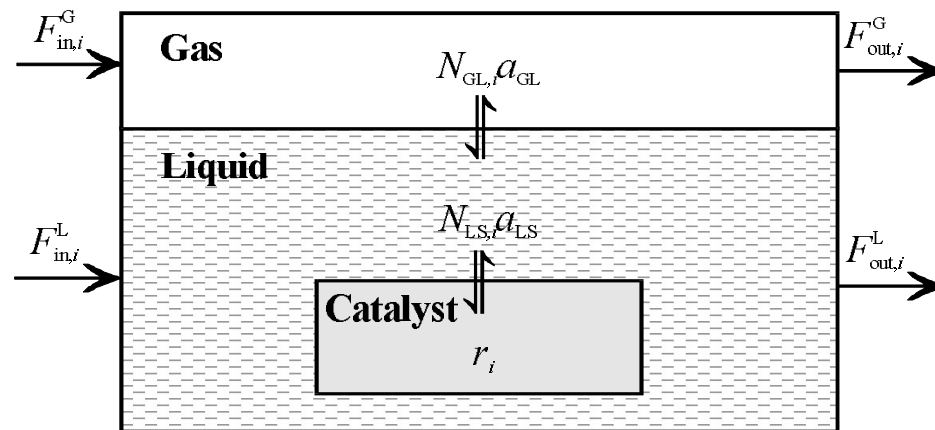


Figure 1. The reactor model applied in the estimation of kinetic parameters.

Inlet flow rates were known (regulated by mass flow controllers), whereas outlet flow rates had to be estimated for use in equations 7 and 8. For this, a P-controller simulation was applied:

$$F_{out,i}^G = K_P (V_{calc,i}^G - V_{exp,i}^G)^2 \quad (9)$$

and

$$F_{out,i}^L = K_P (V_{calc,i}^L - V_{exp,i}^L)^2 \quad (10)$$

where the calculated volumes were obtained using the Soave–Redlich–Kwong (Papers I and II) or Peng–Robinson (Papers IV–VI) equation of state and experimental volumes were determined by step response experiments.

The linear system of ordinary differential equations 7 and 8 was integrated numerically using the Flowbat flowsheet simulator.⁵³ In Papers I,II, and IV, a routine based on the semi-implicit Runge–Kutta method (Stiff 9)⁵⁴ was used. In Papers V and VI, the integrator was developed further in order to minimize the computation time. A hybrid integrator was implemented, which alternated dynamically between two calculation routines: one based on the semi-implicit Runge–Kutta (Stiff 9)⁵⁴ and the other on the Gear and Adams–Moulton method (VODE).⁵⁵

3.3. Minimization of the Objective Function

The objective function to be minimized was the sum of the squares of the differences between the experimental and calculated molar fractions of the liquid product:

$$\text{RSS} = \sum_i (x_{\text{exp},i} - x_{\text{calc},i})^2 \quad (11)$$

Equation 11 was minimized using the Levenberg–Marquardt routine, which was implemented using the in-house parameter estimation program Kinfit.

4. HYDROGENATION OF AROMATIC COMPOUNDS

4.1. Qualitative Hydrogenation Results

Methylcyclohexane was the only observed hydrogenation product of toluene, whereas the hydrogenation of naphthalene gave partly hydrogenated intermediates in addition to the fully hydrogenated *cis*- and *trans*-decahydronaphthalene (decalin). These intermediates were 1,2,3,4-tetrahydronaphthalene (tetralin) and $\Delta^{1,9}$ - and $\Delta^{9,10}$ -octahydronaphthalene (-octalin). A typical product composition of the GC analysis is presented in Figure 2. Tetralin and decalins were the main hydrogenation products, whereas only small amounts of $\Delta^{9,10}$ -octalin (< 0.5 mol %) and traces of $\Delta^{1,9}$ -octalin were observed. The fraction of *cis*-decalin was typically 40% of the decalins virtually regardless of temperature, pressure, or initial concentration. On noble metal catalysts, higher contents of the *cis*-product have been reported.^{56,57} In experiments with pure *cis*- or *trans*-decalin under the same conditions as the other experiments, isomerization was not observed. Therefore it can be concluded that the stereochemistry was governed by chemical kinetics.

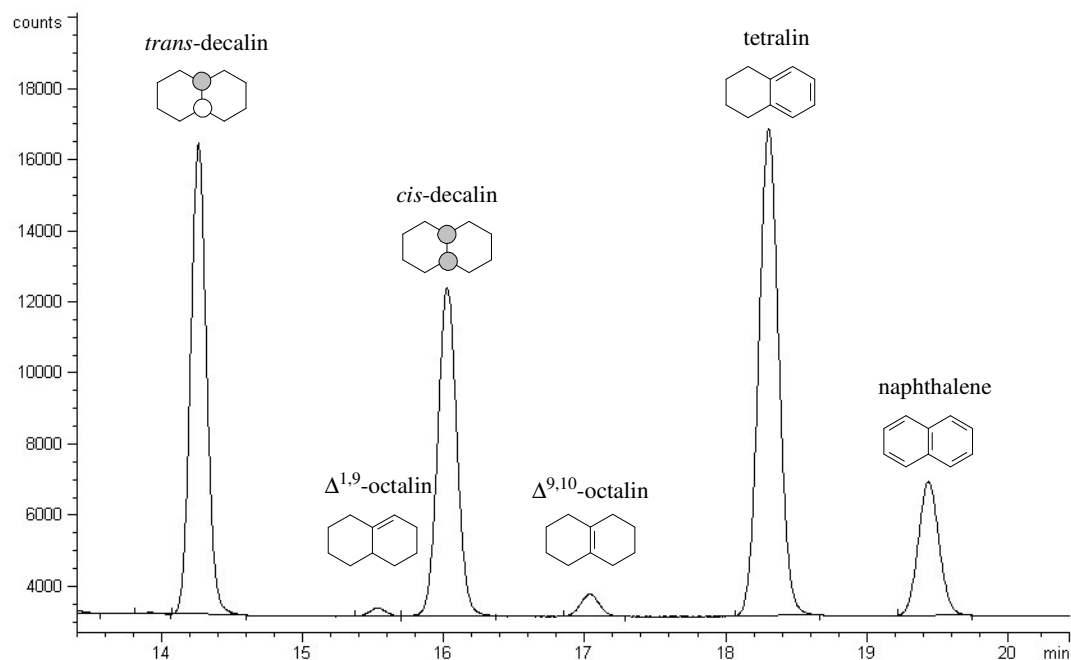


Figure 2. Product composition in the hydrogenation of naphthalene (Paper I).

On the basis of the product compositions, a reaction mechanism was proposed in Paper I for the aromatic model compounds (Figure 3). The mechanism involves

stepwise addition of two hydrogen atoms. This was supported by the observed product compositions, namely the presence of partly hydrogenated intermediates ($\Delta^{1,9}$ - and $\Delta^{9,10}$ -octalin) in tetralin hydrogenation and the formation of tetralin as the sole product in naphthalene hydrogenation at low conversions. The fact that methylcyclohexene was not observed in the hydrogenation of toluene can be explained by kinetic coupling, *i.e.* the high reactivity of methylcyclohexene relative to toluene. Similarly, the reaction mechanism includes the formation of both di- and hexahydronaphthalene. Even though not detected in these studies, the presence of isomers of these intermediates on noble metal catalysts have been reported.⁵⁶

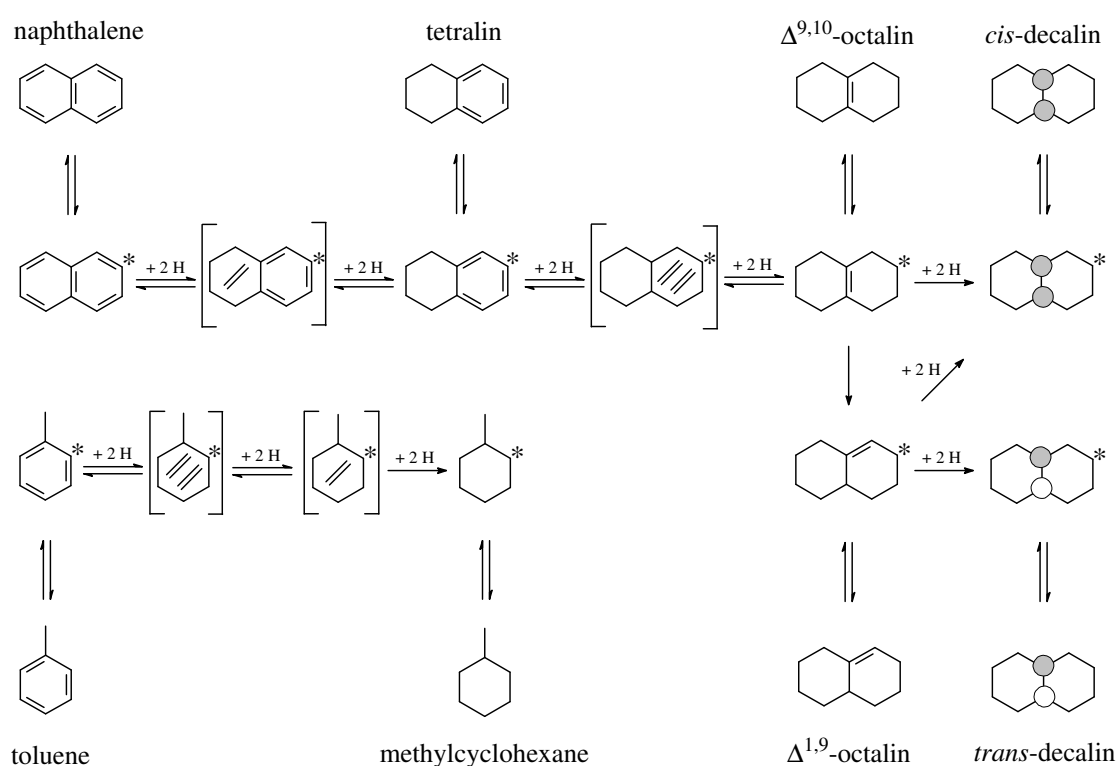


Figure 3. The proposed reaction scheme for the hydrogenation of the aromatic model compounds.

The irreversibility of the reaction from octalins to decalins was deduced from the absence of any traces of octalins when pure *cis*- or *trans*-decalin was fed to the reactor in the normal hydrogenation conditions. Comparison of the hydrogenation rates of octalin isomers on PtO showed that the rate for $\Delta^{1,9}$ -octalin is 25 times that for $\Delta^{9,10}$ -octalin,⁵⁸ and the difference is even higher on reduced noble metals.⁵⁶ Therefore, we

assumed irreversible isomerization from $\Delta^{9,10}$ -octalin to $\Delta^{1,9}$ -octalin and that the main hydrogenation route goes via $\Delta^{1,9}$ -octalin. The fact that the ratio of the octalins was close to 1:1 supports this assumption because the hydrogenation of $\Delta^{9,10}$ -octalin would give *cis*-decalin as the only product. Finally, the high content of *cis*-decalin at the start-up of the experiments implied that hexahydronaphthalene is first hydrogenated to $\Delta^{9,10}$ -octalin, which, after start-up, reacts to decalins for the most part via $\Delta^{1,9}$ -octalin.

The hydrogenation rates of the aromatic model compounds decreased in the following order: naphthalene \gg tetralin $>$ toluene. It seems therefore that the electronic density of the aromatic ring determines the hydrogenation reactivity rather than steric effects. This conclusion is supported by the fact that the first ring of naphthalene, which has the highest C–C bond electron density,⁵⁹ was the most reactive. Furthermore, tetralin was more reactive than toluene despite the larger substituent attached to the aromatic ring of tetralin. These observations are consistent with the reported data according to which the differences in the hydrogenation rates due to steric restraints arising from the size and shape of the alkyl substituents are relatively small.^{60,61}

The reactivity of the model compounds decreased in the same order, regardless of whether they were hydrogenated separately or as mixtures. In mixtures, the hydrogenation rates were, however, affected by the competing reactions. The hydrogenation rates of toluene and tetralin were low when naphthalene was present in the mixture, while the rate of reaction from naphthalene to tetralin was only slightly affected by toluene and tetralin. This was explained in terms of competitive adsorption and subsequent inhibition. Similar observations on the effect of competitive adsorption have been made earlier with mixtures of monoaromatic compounds with different alkyl substituents.¹⁸

4.2. Catalyst Deactivation

Standard periods at the beginning and end of the experiments showed that the catalyst's activity decreased during the experiments, which was assumed to be caused by the formation of hydrogen-deficient species. The benzene ring is known to chemisorb on metal catalysts via its π -bonds such that the plane of the aromatic ring is parallel to the metal surface. Such π -bonded chemisorbed species can lose hydrogen and form less reactive σ -bonded surface species. Further dissociation of these surface

species leads to the formation of coke precursors and loss of the active metal surface.^{62,63} It has been reported that saturated C–H bonds (present in toluene and tetralin but not in naphthalene) are more easily dissociated than the corresponding aromatic bonds.⁶⁴ The results in Papers I and II support this finding in that the deactivation rate was lower with naphthalene as the sole reactant (Paper I) than with multicomponent mixtures (Paper II).

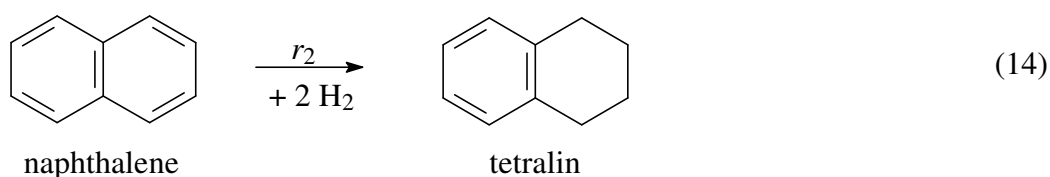
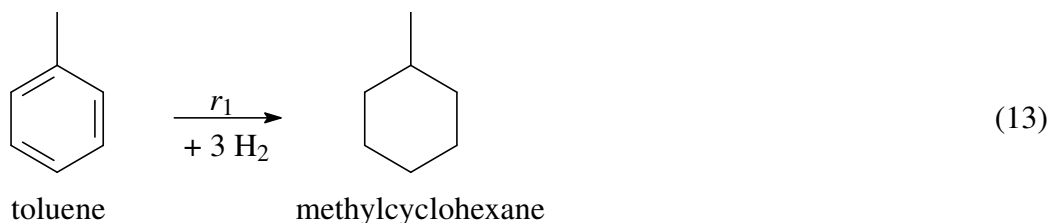
The amount of carbonaceous deposits could not be measured during the experiments, and therefore empirical power-law equations were applied in the modeling of deactivation:

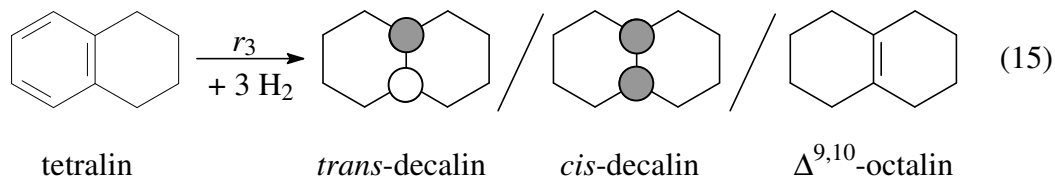
$$-\frac{da}{dt} = k_D a^\delta = A_D \exp\left(-\frac{E_D}{RT}\right) a^\delta \quad (12)$$

In Paper I, the temperature dependence of the deactivation coefficient k_D was observed to be moderate (E_D of about 4 kJ/mol). This encouraged us to assume a deactivation coefficient independent of temperature in Paper II.

4.3. Hydrogenation Kinetics

The reaction scheme presented in Figure 3 was simplified in order to reduce the number of kinetic parameters and thus avoid excess correlation. Since quantitative determination of $\Delta^{1,9}$ -octalin was not possible with the methods of analysis applied, this isomer was excluded from the kinetic model and decalins, together with $\Delta^{9,10}$ -octalin, were described as one pseudo-component. Consequently, the reaction schemes in Papers I and II could be described by three rate equations for the conversions toluene to methylcyclohexane (13), naphthalene to tetralin (14), and tetralin to the combined products ($\Delta^{9,10}$ -octalin, *cis*-, and *trans*-decalin) (15):





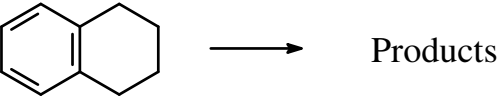
The hydrogenation kinetics of the reactions (equations 13–15) were described by the generalized Langmuir–Hinshelwood equations³⁰

$$-r_i = \frac{k_i c_i^{m_i} c_H^{m_H}}{\left[1 + \sum_j (K_j c_j)^{m_j} \right]^l} \quad (16)$$

in which the temperature dependencies of the rate and adsorption equilibrium constants were described with the Arrhenius and van't Hoff equations, respectively. In Paper II, because of the complex nature of the reaction system, in which three model compounds were hydrogenated simultaneously, it was assumed that the reaction orders with respect to the two monoaromatic compounds were the same, and that the orders with respect to hydrogen in each of the reactions were also the same. Furthermore, in Paper II, the adsorption enthalpy of the aromatics and hydrogen was assumed to be zero. This simplification was supported by the estimated low values for ΔH_{ads} (< 9 kJ/mol for naphthalene, tetralin, and hydrogen) in Paper I. The weak temperature dependence of the adsorption parameters can probably be explained in terms of the high surface concentrations associated with reactions in the liquid phase. Adsorption enthalpy is known to decrease as the surface coverage increases,⁶⁵ and the temperature dependence of K_i is therefore quite often ignored in the modeling of liquid-phase hydrogenation reactions.^{66–68}

Parameter estimation results showed that the reaction rate constants and adsorption equilibrium constants increase with reactivity in both Paper I and Paper II (naphthalene > tetralin > toluene). This is consistent with the qualitative observations in that the most reactive component adsorbs most strongly on the catalyst and thus inhibits the other reactions. Relative hydrogenation rates (free of mass-transfer effects) of the model compounds are presented at two temperatures in Table 4. The rates are calculated with the kinetic parameters from Paper II and correspond to the experiment in which the hydrogen pressure was 20 bar and the feed contained 20 mol % of toluene, 10 mol % of tetralin, and 6 mol % of naphthalene in n-decane.

Table 4. Relative hydrogenation rates of the aromatic model compounds.

Reaction	Relative rate	
	80 °C	140 °C
	1.0	22
	69	150
	2.5	38

The adsorption equilibrium constants of both tetralin and naphthalene were of the same order of magnitude, regardless of whether they were estimated from single- or multicomponent data. At the average temperature (110 °C) the values of the adsorption parameters were $5.2 \times 10^{-3} \text{ m}^3/\text{mol}$ for naphthalene and $3.2 \times 10^{-3} \text{ m}^3/\text{mol}$ for tetralin in Paper I, compared with the values $7.8 \times 10^{-3} \text{ m}^3/\text{mol}$ (naphthalene) and $4.4 \times 10^{-3} \text{ m}^3/\text{mol}$ (tetralin) in Paper II. For toluene, the estimated values differed markedly, however. In the single-compound and mixture models, K_{toluene} had the values of $1.1 \times 10^{-4} \text{ m}^3/\text{mol}$ ⁶⁹ and $1.0 \times 10^{-3} \text{ m}^3/\text{mol}$ (Paper II), respectively. The possible reason for this large difference is that in the study with pure toluene,⁶⁹ ideal Langmuir adsorption was assumed in the formulation of the kinetic equations. However, as the high reaction order toward toluene (1.43) in mixture models (generalized Langmuir–Hinshelwood equations) indicates this assumption is most likely not well founded, and the physical meaning of the corresponding parameters is uncertain.

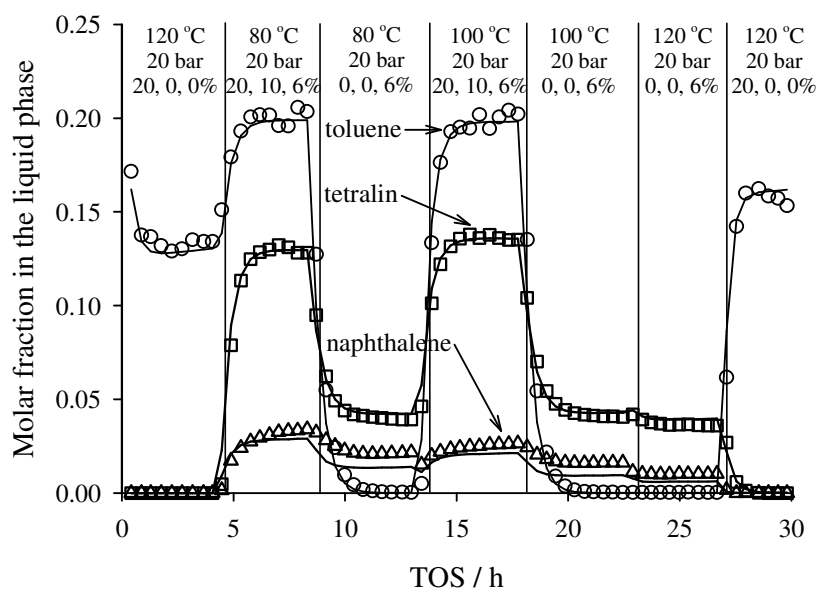
The estimated activation energies of toluene and tetralin were rather close to one another in the single-compound and multicomponent hydrogenation experiments. The estimated values for toluene were 49 kJ/mol⁶⁹ and 53 kJ/mol (Paper II), and for tetralin 41 kJ/mol (Paper I) and 40 kJ/mol (Paper II). These values are also well in

accordance with other gas- and liquid-phase hydrogenation studies.^{6,13,14} However, the estimated activation energies for naphthalene in Papers I and II differ significantly from one another. A value of 26 kJ/mol was estimated from the data when naphthalene was hydrogenated separately, whereas a value of 59 kJ/mol was estimated when naphthalene was hydrogenated in aromatic mixtures. The difference was more likely caused by uncertainties in the parameter estimation than by physical differences in the reaction systems, because naphthalene content was typically low in the product streams, which made its error least significant in the objective function.

4.4. Validation of the Kinetic Models

Competitive adsorption between different aromatics complicates the scale-up and optimization of dearomatization reactors (trickle beds) because, as was seen in the present study, the rates in mixtures differ from the rates when the same compounds are hydrogenated separately. In Paper II it was examined whether these mixture effects can be modeled simply by applying kinetic equations from the single-compound experiments and describing the competitive adsorption according to the Langmuir–Hinshelwood equations. For this, experiments with multicomponent feeds were simulated using the kinetic equations and parameter values from Paper I for the hydrogenation of naphthalene and tetralin, and earlier published models for the hydrogenation of toluene.⁶⁹ The rates predicted by these models agreed rather well with the rates recorded experimentally in mixtures, if the surface concentration terms $K_i c_i$ for all the aromatics, were included. This can be seen from Figure 4, which shows the results of a kinetic experiment with multicomponent aromatic feeds. The outlet composition is almost equally well predicted by the single-compound based models ($RSS = 1.0 \times 10^{-2}$) as by the mixture models ($RSS = 0.74 \times 10^{-2}$). The difference is small considering that this particular experiment was used in the parameter estimation of the mixture models, whereas the parameters of the single-compound models were estimated independently. Thus we conclude that models based on laboratory experiments with single model compounds are applicable in the simulation of aromatic mixtures if excessive correlation in parameter estimation is avoided and all parameters, especially adsorption equilibrium constants, have physically meaningful values.

**mixture
model**



**single-
compound
models**

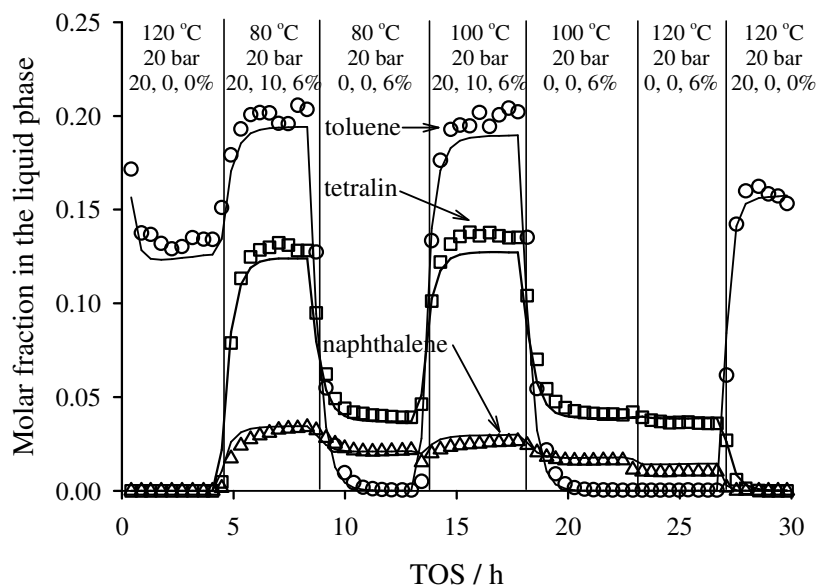


Figure 4. Experimental (open symbols) and calculated (solid lines) molar fractions of toluene, tetralin, and naphthalene in a typical kinetic experiment according to the mixture and single-compound models. The feed composition (mol %) is shown at the top of the graphs in the order (1) toluene, (2) tetralin, and (3) naphthalene.

5. HYDROGENATION OF ISOCTENES

5.1. Thermodynamic Equilibrium between Isooctenes

It is essential to know the thermodynamic equilibrium composition of the isooctene mixture in order to distinguish between the hydrogenation and isomerization kinetics. Therefore, the equilibrium composition of mixtures of TMP-1 and TMP-2 was determined prior to the hydrogenation experiments in a temperature range of 50–100 °C (Paper III). Contrary to the general rule for alkene stability, an excess of α -alkene (TMP-1) was observed. The experimentally determined reaction enthalpy and entropy for the isomerization of TMP-1 to TMP-2 were 3.51 ± 0.03 kJ/mol and -0.47 ± 0.10 J/(mol K), respectively. Thus, in the temperature interval used, the ratio of TMP-1 to TMP-2 varied between 4.1 (50 °C) and 3.4 (100 °C).

5.2. Qualitative Hydrogenation Results

Qualitatively the hydrogenation of isooctenes proceeds in the same way on the applied platinum, nickel, and cobalt catalysts in that isooctane was the sole product and the hydrogenation rate of TMP-1 to isooctane was higher than that of TMP-2 on each catalyst. For example, in the first standard period of the experiments with Pt (100 °C, 20 bar, 5 mol % isooctene equilibrium mixture in cyclohexane) the conversions with respect to TMP-1 and TMP-2 were 32% and 14%, respectively. The rate of TMP-1 relative to TMP-2 was similar on the other two catalysts. The overall conversions were 3–40% (WHSV \approx 1400 h⁻¹) on Ni, 4–55% (WHSV \approx 330 h⁻¹) on Co, and 6–60% (WHSV \approx 200 h⁻¹) on Pt. Comparison of the observed rates is, however, not straightforward because of the different conditions and particle size for Pt.

Double bond shift isomerization between TMP-1 and TMP-2 had no importance in the applied reaction conditions on any of the catalysts. This was verified with experiments where either pure TMP-1 or TMP-2 was used as the reactant. The amount of isomerization product (TMP-1 or TMP-2) in these experiments was always low. For example, the feed that contained 5 mol % of TMP-2 resulted in a TMP-1 (isomerization product) concentration of only 0.3 mol % at 140 °C and 20 bar on Pt, whereas the concentration of isooctane (hydrogenation product) was 5 times greater. Slow double-bond isomerization in the liquid-phase hydrogenation of 1-butene on

Pt/Al₂O₃ has been reported,⁷⁰ and the present study showed a similar trend for Ni and Co catalysts. However, Pecque and Maurel observed that isomerization does play an important role in the hydrogenation of TMP-1 and TMP-2, when the pure isomers are used as reactants on Raney nickel at 25 °C and under 1.0 bar hydrogen pressure.⁷¹ The most likely explanation for this dissimilarity is the different conditions under which the experiments were performed. Since the hydrogenation rates increase faster than the isomerization rate with hydrogen pressure, it is expected that the role of isomerization will be less pronounced at elevated pressures than at ambient pressure.

5.3. Catalyst Deactivation

Catalyst deactivation during the experiments was observed on all the catalysts. Deactivation was assumed to be due to the formation of hydrogen-deficient species. On Ni and Co the original activity was completely recovered by flushing the used catalyst with hydrogen at 400 °C, whereas on Pt such regeneration was not observed. In addition, the deactivation rate was the highest on Pt. After the typical 30-h runs, the activity on Pt was less than 20% of the original, compared to the values of 80% on Ni and 55% on Co. This is illustrated in Figure 5, where the formation rates of isooctane during the first and last standard periods are plotted.

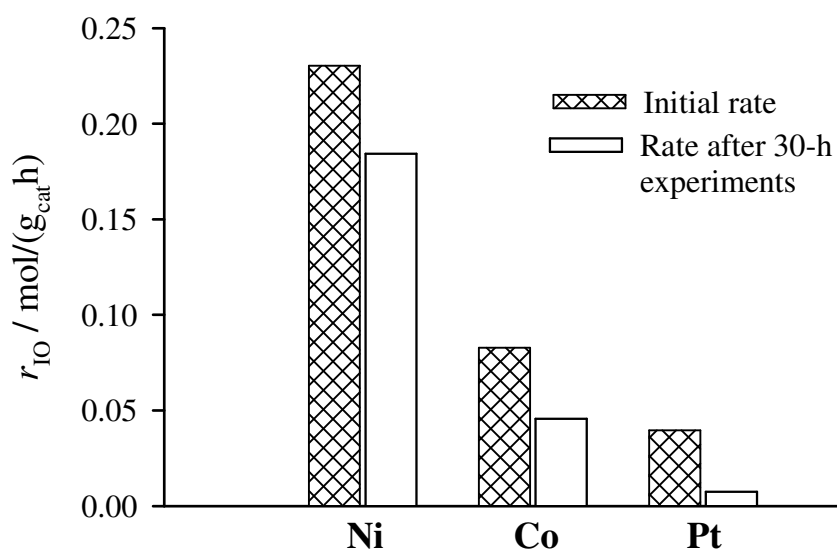


Figure 5. Initial formation rate of isooctane and rate at the end of typical 30-h experiments. Feed: 5 mol % of isooctenes in cyclohexane, $p = 20$ bar, and $T = 75$ °C (Ni, Co) and 100 °C (Pt).

No tools were available for the quantitative analysis of the carbonaceous residue, and therefore the effect of catalyst deactivation was eliminated from the results by the empirical first order equation:

$$-\frac{da}{dt} = k_D a \quad (17)$$

Because temperature had no notable effect on the deactivation rate, the deactivation rate constant k_D was assumed to be independent of temperature on all catalysts. However, on Pt a correlation between the feed composition and deactivation rate was observed in that on increasing the alkene to hydrogen ratio, the deactivation rate also increased. This can be seen in Figure 6, where the formation rates of isooctane in two typical kinetic experiments are shown. In addition, average hydrogen to alkene molar ratios during the second and third periods is indicated by the numerical values. A lower H_2 /alkene-ratio leads to more severe deactivation (more significant decline in the rate) during these periods, as can be seen in the right hand side of Figure 6.

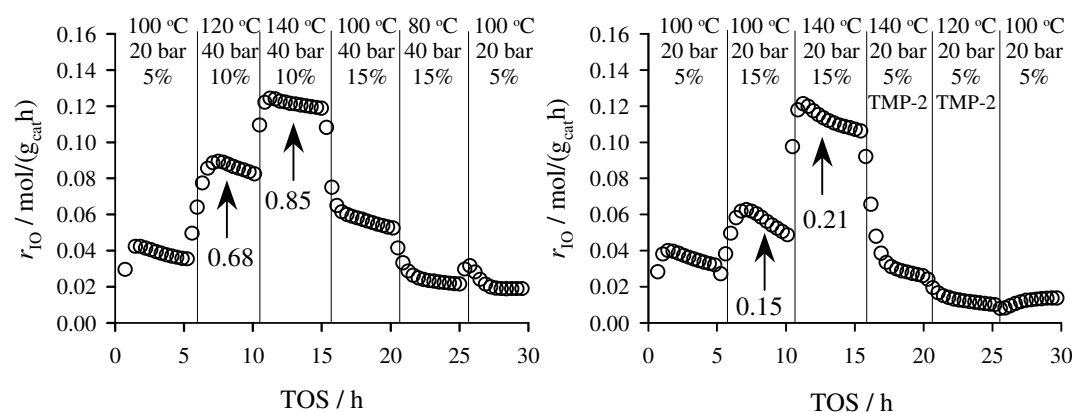


Figure 6. The results of two typical kinetic experiments to measure the formation rate of isooctane in the hydrogenation of TMP-1 and TMP-2 on Pt/Al₂O₃.

On Pt, due to the dependence of the deactivation rate on the reaction mixture composition, k_D was described in Paper VI according to

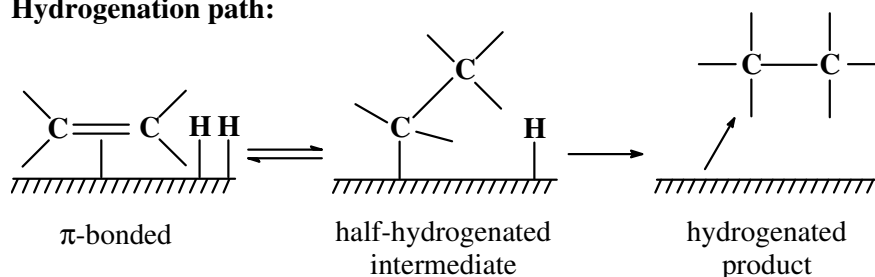
$$k_D = k_{D,0} \left(\frac{c_{\text{TMP-1}} + c_{\text{TMP-2}}}{c_H} \right)^d \quad (18)$$

Thus the deactivation model in Paper VI included two parameters: $k_{D,0}$ and d .

It is reported that the main path in the hydrogenation involves π -bonded alkene, which is bonded to a single Pt atom.^{22,23} The reactions of the π -bonded alkene to the di- σ -bonded form and then to ethylidyne through cleavage of one hydrogen atom, are

much slower than the hydrogen addition to the π -bonded alkene and can eventually lead to catalyst deactivation as ethynyl species polymerize to form hydrogen-deficient species.⁷² Therefore, the hydrogenation and deactivation mechanisms presented in Figure 7 were presumed.

Hydrogenation path:



Deactivation path:

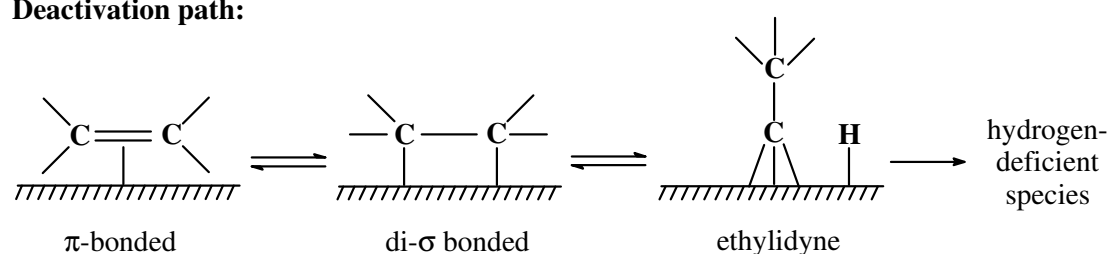


Figure 7. Proposed hydrogenation and deactivation mechanism in the hydrogenation of TMP-1 and TMP-2.

5.4. Hydrogenation Kinetics

In this work, it was presumed a hydrogenation mechanism that involves π -adsorbed alkene to which dissociatively adsorbed H atoms are inserted in two consecutive steps (Figure 7). In Figure 8 the proposed mechanism is applied to hydrogenation of TMP-1 and TMP-2. It was assumed that the double bond isomerization between TMP-1 and TMP-2 takes place via a common half-hydrogenated intermediate (Y). Isomerization experiments (Paper III) supported this assumption, in that a strongly acidic ion-exchange resin (H^+ 5.2 equiv/kg) was needed in order to establish the equilibrium between TMP-1 and TMP-2, whereas in the absence of either hydrogen or acid sites, the equilibration did not occur. The observed slow isomerization rate compared to the hydrogenation rates suggests rate limitation by the first rather than the second hydrogen addition. Rate limitation by the second hydrogen addition is associated with equilibrium in the formation of the half-hydrogenated intermediate and a high isomerization rate, contrary to our findings.

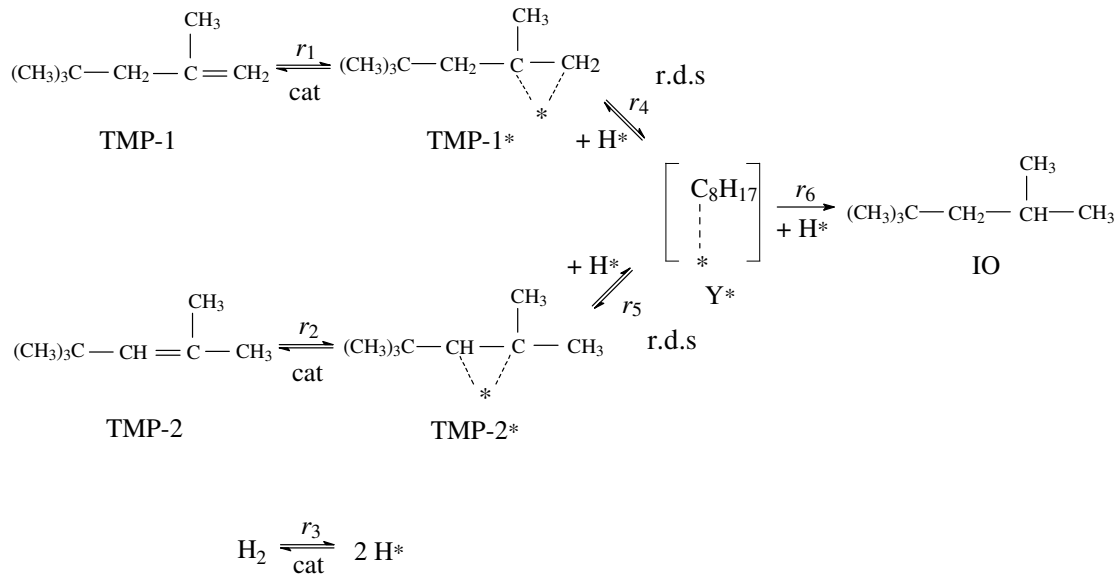


Figure 8. Proposed mechanism for the hydrogenation of TMP-1 and TMP-2.

The following equations can be derived for TMP-1 and TMP-2 from the mechanism presented in Figure 8, if the first hydrogen addition is assumed to be the rate-limiting step:

$$-r_i = \frac{k_i c_i \sqrt{c_H}}{\left(1 + \sum_{i=1}^2 K_i c_i + \sqrt{K_H c_H}\right)^2} \quad (19)$$

and

$$-r_i = \frac{k_i c_i \sqrt{c_H}}{\left(1 + \sum_{i=1}^2 K_i c_i\right) \left(1 + \sqrt{K_H c_H}\right)} \quad (20)$$

Equations 19 and 20 correspond to the competitive and non-competitive adsorption of the alkenes and hydrogen, respectively. Because rate limitation was assumed by the first hydrogen addition, both models reduce to the form with no rate constants for either reversible reactions or equilibrium constant between TMP-1 and TMP-2. The observed slow isomerization on all catalysts supported this assumption (see section 5.2). Temperature dependence within the rate equations was expressed completely by the rate constants k_i , which were described using the Arrhenius law and apparent

values for the activation energies. The adsorption constants K_i were assumed to be independent of temperature under the conditions used in this study.

Furthermore, power-law models were applied to the modeling of kinetic data on the Co/SiO₂ catalyst in Paper V. The results showed that the reaction orders with respect to the alkenes and hydrogen were 0.38 and 0.43, respectively. However, the mechanistic models expressed by equations 19 and 20 were preferred over the power-law equations, because they described the experimentally recorded data as well. Parameters with a physical meaning probably give a better fit, if the models are extrapolated outside the conditions used in the present study. The estimated values of the kinetic parameters for the competitive adsorption model (equation 19) are presented in Table 5 for all the catalysts tested, and examples of the corresponding model fits in Figure 9. The competitive and non-competitive adsorption models resulted in very similar fits, and therefore discrimination between the adsorption mechanisms can not be made on the basis of statistical analysis.

Table 5. Kinetic parameters and 95% confidence intervals in the hydrogenation of TMP-1 and TMP-2, competitive adsorption model (equation 19).

	Ni/Al ₂ O ₃	Co/Al ₂ O ₃	Pt/Al ₂ O ₃
$k_{ref,TMP-1} \times 10^4$ / mol/(g _{cat} h) (m ³ /mol) ^{3/2}	5.1 ± 0.2 ^a	1.6 ± 0.1 ^a	3.2 ± 0.1 ^b
$k_{ref,TMP-2} \times 10^4$ / mol/(g _{cat} h) (m ³ /mol) ^{3/2}	2.2 ± 0.3 ^a	0.37 ± 0.02 ^a	0.64 ± 0.02 ^b
$E_{app,TMP-1}$ / kJ/mol	34 ± 2	35 ± 1	49 ± 1
$E_{app,TMP-2}$ / kJ/mol	49 ± 6	43 ± 2	65 ± 2
$K_{TMP-1} \times 10^4$ / mol/m ³	6.0 ± 0.5	13.0 ± 0.5	18.8 ± 0.7
$K_{TMP-2} \times 10^4$ / mol/m ³	1.8 ± 0.3	3.8 ± 0.2	13.0 ± 0.3
$K_H \times 10^4$ / mol/m ³	0.16 ± 0.03	0.30 ± 0.01	38 ± 1

^a Reference temperature 65 °C. ^b Reference temperature 110 °C.

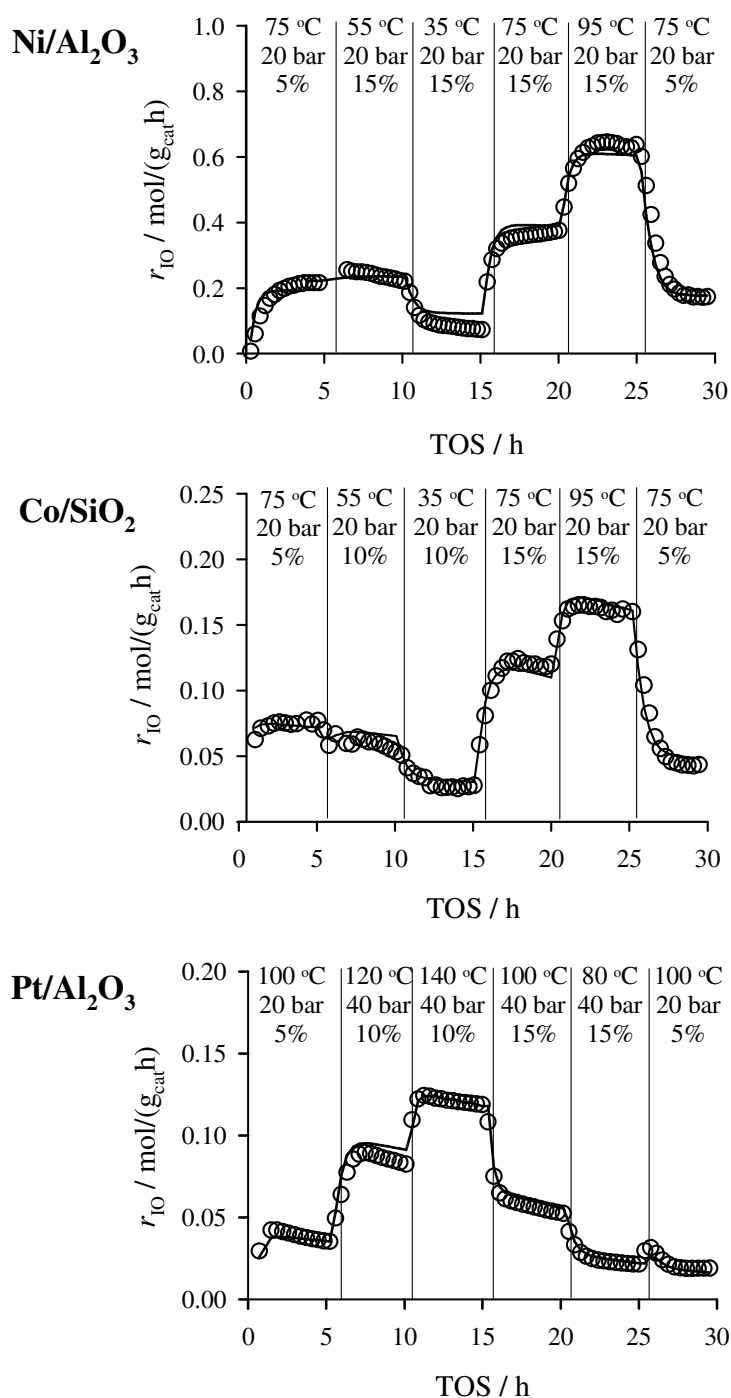


Figure 9. Examples of the model fit in the hydrogenation of TMP-1 and TMP-2 on the Ni/Al₂O₃, Co/SiO₂, and Pt/Al₂O₃ catalysts. Open circles and continuous lines correspond to the experimental and calculated rates, respectively.

The parameter values in Table 5 show some common trends on all the catalysts tested. The estimated rate and adsorption equilibrium constants of TMP-1 were higher than those of TMP-2, implying a stronger adsorption and a higher hydrogenation

reactivity for TMP-1. Additionally, the activation energy of TMP-2 relative to TMP-1 is higher on each catalyst. These effects are probably caused by steric hindrance by the *tert*-butyl group that is closer to the C–C double bond in TMP-2 than in TMP-1. In addition to the steric effects, electron donation by the *tert*-butyl group into the activated complex can contribute to the lower reactivity of TMP-2. The complex for TMP-2 will be less stable than that for TMP-1 because in TMP-1 the –CH₂– group distances the *tert*-butyl group from the unpaired electrons. Electronic substituent effects on the bond order⁷³ and on the hydrogenation rate of alkene double bonds⁷⁴ have been reported to be rather small, however, and it appears therefore that the lower reactivity of TMP-2 is mostly attributable to the steric effects.

Despite the above mentioned common trends, platinum differs from nickel and cobalt in the magnitude of activation energies. E_{app} values for both isomers are higher on Pt (48–49 kJ/mol for TMP-1 and 64–65 kJ/mol for TMP-2) than on Ni or Co (34–35 kJ/mol for TMP-1 and 40–48 kJ/mol for TMP-2). These parameters are in a physically meaningful range,⁷⁵ and they also agree with the reported data for the double-bond hydrogenation on nickel.^{67,76} Activation energies on platinum are, however, somewhat higher in the work presented here than in other studies found in the literature (25–37 kJ/mol).^{77–79} No literature values for the hydrogenation of alkene double bonds on cobalt could be found.

However, the most significant difference in the parameters between different catalysts is found in K_H , which has the value of 0.16×10^{-4} m³/mol on Ni/Al₂O₃, 0.30×10^{-4} m³/mol on Co/SiO₂, and 38×10^{-4} m³/mol on Pt/Al₂O₃. The two orders of magnitude higher adsorption equilibrium constant on Pt corresponds to the higher hydrogen surface coverage on Pt. The calculated hydrogen coverages are 3–6% (Ni), 3–8% (Co), and 21–46% (Pt) in the applied conditions. Despite this, deactivation through the formation of carbonaceous deposits was the fastest on Pt. There are two reasonable explanations for this seemingly inconsistent result:

i) The low metal content and small number of active sites make the Pt catalyst more sensitive to deactivation due to carbonaceous deposits. The number of active sites (determined by hydrogen chemisorption) decreases in the same order as the deactivation rate increases: Ni/Al₂O₃ (2.7×10^{20} atoms/g_{cat}), Co/SiO₂ (3.5×10^{19} atoms/g_{cat}), and Pt/Al₂O₃ (8.8×10^{18} atoms/g_{cat}). Additionally, because the rate per active site (turnover frequency, TOF) is approximately the same (Figure 10), the

number of active sites seems to explain the differences in activity between these catalysts.

ii) More strongly bonded and less mobile reaction intermediates on Pt, as indicated by the higher activation energies, are more susceptible to losing hydrogen and forming ethylidyne species and therefore carbonaceous residue. This assumption is supported by the fact that the TOF values are not higher on Pt than on Ni or Co even though the calculated surface concentrations of the reactants are the highest.

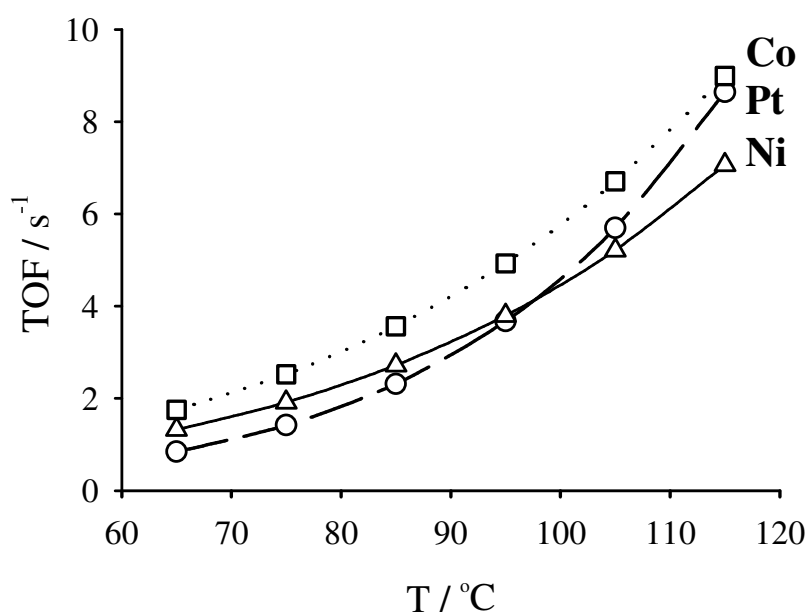


Figure 10. Turnover frequencies (TOFs) on different catalysts as a function of temperature ($c_{\text{TMP-1}} = 500 \text{ mol/m}^3$, $c_{\text{TMP-2}} = 150 \text{ mol/m}^3$, $c_{\text{H}} = 200 \text{ mol/m}^3$). Figure taken from Paper VI.

5.5. Usability of Ni, Co, and Pt Catalysts on the Industrial Scale

All tested catalysts were active and selective in the hydrogenation of TMP-1 and TMP-2. Therefore, any of them could in principle be applied to the industrial-scale. However, differences between the studied catalysts arise from different activity, price, and deactivation rate. Nickel was the most active of the studied catalysts, and deactivation caused by the carbonaceous deposits was the least. Also, nickel catalysts are inexpensive, especially compared to the noble metals. The problem with nickel is its low resistance towards sulfur and nitrogen compounds.^{72,80} These compounds form nickel sulfide and nitride, which are considerably less active in hydrogenation, and the regeneration of the poisoned catalysts is usually not possible. Cobalt is also cheaper

than the noble metals, but it suffers from the same problem as nickel in that sulfur and nitrogen compounds deactivate it rapidly.⁷² Also, the active surface area (reducibility/dispersion) is lower than on Ni, which leads to lower reaction rates. Pt requires higher temperatures and deactivates due to the formation of carbonaceous deposits. It is, however, more resistant towards sulfur impurities. For the liquid-phase hydrogenation of isooctenes, it has been suggested that for feeds with less than 1 ppm of sulfur, nickel is a better choice, but if more sulfur is present (1–10 ppm), a noble metal catalyst should be used.⁸¹ However, it is possible to significantly improve sulfur resistance of Ni and Co catalysts with catalyst additives such as Mo and B which selectively adsorb sulfur.⁷²

From the present study and the reports referred to above, it is concluded that nickel is the best catalyst to use with sulfur-free feeds. Likewise, in the presence of sulfur, either Ni or Pt (or other noble metal) should be chosen depending on the precise nature of the impurities in the industrial application.

6. COMMON FEATURES IN HYDROGENATION

For both the aromatics and alkenes, a mechanism of stepwise addition of dissociatively adsorbed hydrogen was proposed. This mechanism includes formation of cycloalkenes as intermediates in the hydrogenation of aromatic compounds. Indeed, cycloalkenes ($\Delta^{1,9}$ - and $\Delta^{9,10}$ -octalin) were observed in the product mixtures in addition to the fully saturated products. The amounts of these intermediates were very small, however, which was explained in terms of kinetic coupling caused by high reactivity of the cycloalkenes compared with the aromatic compounds. This assumption is supported by the fact that on the nickel catalyst the hydrogenation rates of the alkenes (TMP-1 and TMP-2) were higher by two orders of magnitude than the rates of the monoaromatic compounds. For example, the turnover frequency (TOF) in the formation of methylcyclohexane from toluene was $3.0 \times 10^{-2} \text{ s}^{-1}$ compared with the value of 4.6 s^{-1} in the formation of isooctane from isooctene under the same conditions ($T = 100 \text{ }^\circ\text{C}$, $c_i = 700 \text{ mol/m}^3$, $c_{\text{H}} = 200 \text{ mol/m}^3$). Additionally, the slow double-bond isomerization in the hydrogenation of TMP-1 and TMP-2 indicates that the addition of the first hydrogen atom is the rate-determining step in the hydrogenation of alkene double bonds.

All catalysts (Ni, Co, and Pt) deactivated during the kinetic experiments. This was assumed to be due to accumulation of carbonaceous deposit on the active sites. Deactivation on the nickel catalyst was very similar both in the hydrogenation of aromatics and alkenes. In the study with TMP-1 and TMP-2, we compared different catalyst materials and found that deactivation rate increases in the same order as hydrogenation rate decreases: 1) Ni, 2) Co, and 3) Pt. This was mostly attributable to the differences in the number of active sites: the higher the number of sites the higher the reaction rate and better the resistance towards the formation of carbonaceous impurities. Despite the different deactivation rates, carbonaceous residue was assumed to be responsible for the loss of catalytic activity on Co and Pt, similarly with Ni. Evidence of this was obtained on Pt, where the hydrogen to alkene ratio had an appreciable effect on the deactivation rate. A low H_2 /alkene ratio caused more severe deactivation than a high one.

External mass-transfer limitations (G–L and L–S) could be eliminated in the CSTR experiments by efficient mixing in the hydrogenation of both aromatics and

alkenes. This is favorable, because simultaneous modeling of several phenomena induces uncertainties in the parameter optimization. Internal diffusion limitations could not be avoided, however. Even in the case of aromatic model compounds, whose reaction rates were considerably slower than that of the alkenes, the observed rates were subject to pore diffusion resistance with the particle size used (0.5 mm). Therefore it seems that on the industrial scale, where a large particle size must be used in order to minimize the pressure drop over fixed catalyst beds all the reactions described in this thesis occur under severe internal diffusion limitation. In the reactor design, internal diffusion must be described separately from the chemical kinetics by calculating mole balances inside the catalyst particle. These calculations should be carried out considering both diffusion (with effective diffusion coefficients) and the intrinsic rates of chemical reactions.

To summarize, a very similar approach was suitable for both the aromatics and alkenes with regard to experimental work and kinetic modeling.

7. CONCLUSIONS

The hydrogenation of both the aromatic and alkene compounds presented in these studies was presumed to follow a stepwise addition mechanism of dissociated hydrogen atoms. Corresponding Langmuir–Hinshelwood type rate equations were used to describe the reaction kinetics accurately with physically meaningful and well identified parameter values. It appears that the relative rates of the aromatic model compounds (toluene, tetralin, and naphthalene) are mainly governed by electronic rather than by steric effects in that the first ring of the diaromatic compound (naphthalene), which has the highest electron density of the compounds studied, was far more reactive than the monoaromatic model compounds (toluene and tetralin). Furthermore, tetralin was more reactive than toluene despite the more bulky cyclic substituent attached to its aromatic ring. The experiments with the branched alkenes showed, however, that steric effects can also affect the hydrogenation reactivity. The large *tert*-butyl substituent next to the double bond in TMP-2 makes it considerably less active than TMP-1 in adsorption and hydrogenation, even though the electron density in the double bonds of these isomers is not expected to vary appreciably.

In the study with the aromatic model compounds it was shown that hydrogenation kinetics in multicomponent mixtures can be described with rate equations based on single-compound experiments if the adsorption equilibria of all aromatics are included in the rate equations. Single-compound models are thus possibly applicable in the simulation of dearomatization of real diesel fractions.

Similar experimental setup and calculation methods were suitable for both the aromatics and alkenes. The test reactor's continuous operation together with the standard periods at the beginning and the end of the experiments, enabled the effect of catalyst deactivation on the chemical kinetics to be eliminated. This is scarcely possible with batch reactor methods. Furthermore, since the effects of mass transfer and the reaction matrix (hydrogen solubility) on the observed rates were eliminated in the optimization of kinetic parameters, the obtained models are applicable to process simulators.

8. LIST OF ABBREVIATIONS AND SYMBOLS

A_D	frequency factor for the catalyst decay, s^{-1}
a_{GL}	gas–liquid mass-transfer area / reactor volume, m^{-1}
a_{LS}	liquid–solid mass-transfer area / reactor volume, m^{-1}
A_p	surface area of a catalyst particle, m^2
B	shape factor of a catalyst particle
c_i	concentration, mol/m^3
c_p	heat capacity of a catalyst particle, $J/(g\ K)$
CSTR	continuous stirred tank reactor
d	parameter in equation 18
D	molecular diffusion coefficient, m^2/s
D_{eff}	effective diffusion coefficient, m^2/s
E_{app}	apparent activation energy, kJ/mol
E_D	activation energy for the catalyst deactivation, kJ/mol
F	molar flow rate, mol/s
GC	gas chromatography
ΔH_{ads}	adsorption enthalpy, kJ/mol
ΔH_R	reaction enthalpy, kJ/mol
k	rate constant, unit dependent on the form of the rate equation
K	adsorption equilibrium constant, mol/m^3
k_D	deactivation rate constant, s^{-1}
$k_{D,0}$	parameter in equation 18, s^{-1}
K_{GL}	vapor–liquid equilibrium constant
K_P	constant in equations 9 and 10, $mol/(m^6\ s)$
k_t	thermal conductivity of the catalyst particle, $W/(m\ K)$
l	parameter in equation 16
m	parameter in equation 16
n	amount, mol
N_{GL}	flux at the gas–liquid interface, $mol/(m^2\ s)$
N_{LS}	flux at the liquid–solid interface, $mol/(m^2\ s)$
PAH	polyaromatic hydrocarbon
PR	Peng–Robinson equation of state

r_i	reaction rate of compound i, mol/(g _{cat} h)
r_p	radius of a catalyst particle, m
RSS	residual sum of squares (object function)
SRK	Soave–Redlich–Kwong equation of state
t	time, s
T	temperature, K
V_p	volume of a catalyst particle, m ³
V_R	reactor volume, m ³
x	molar fraction in the liquid phase

Sub- and Superscripts

calc	calculated (modeled)
exp	experimental
G	gas phase
H	hydrogen
IO	isooctane (2,2,4-trimethylpentane)
L	liquid phase
R	reactor
TMP-1	2,4,4-trimethyl-1-pentene
TMP-2	2,4,4-trimethyl-2-pentene

Greek Letters

δ	parameter in equation 12
ε	porosity
Φ	Weisz–Prater criterion
κ	mass-transfer coefficient, m/s
λ	dimensionless position within a catalyst particle
ρ	density, kg/m ³
τ	tortuosity factor

9. REFERENCES

1. Allen, L.; Suchanek, A. Consider the Options for Meeting Stringent European Gasoline Specifications. *Hart's Fuel Technol. Manage.* **8**(2) (1998) 14–16.
2. Hunter, M.; Gentry, A.; Lee, S.; Groeneveld, L.; Olivier, C.; Pappal, D. MAKFining – Premium Distillates Technology: The Future of Distillate Upgrading. Presented at the NPRA 2000 Annual Meeting, San Antonio, TX, Mar 26–28, 2000; Paper AM-00-18.
3. Karonis, D.; Lois, E.; Stournas, S.; Zannikos, F. Correlations of Exhaust Emissions from a Diesel Engine with Diesel Fuel Properties. *Energy & Fuels* **12** (1998) 230–238.
4. Wang, S.-X.; Shao, M.; Zhang, Y.-H. Influence of Fuel Quality on Vehicular NO_x Emissions. *J. Environ. Sci.* **13** (2001) 265–271.
5. Quality of European Gasoline and Diesel Fuels. EU Fuels Directive 2003/17/EC. Mar 3, 2003.
6. Van Meerten, R. Z. C.; Coenen, J. W. E. Gas Phase Benzene Hydrogenation. *J. Catal.* **46** (1977) 13–24.
7. Mirodatos, C.; Dalmon, J. A.; Martin, G. A. Steady-State and Isotopic Transient Kinetics of Benzene Hydrogenation on Nickel Catalysts. *J. Catal.* **105** (1987) 405–415.
8. Franco, H. A.; Phillips, M. J. Gas Phase Hydrogenation of Benzene on Supported Nickel Catalyst. *J. Catal.* **63** (1980) 346–354.
9. Lindfors, L. P.; Salmi, T. Kinetics of Toluene Hydrogenation on a Supported Nickel Catalyst. *Ind. Eng. Chem. Res.* **132** (1993) 34–42.
10. Toppinen, S.; Rantakylä, T.-K.; Salmi, T.; Aittamaa, J. Kinetics of the Liquid-Phase Hydrogenation of Benzene and Some Monosubstituted Alkylbenzenes over a Nickel Catalyst. *Ind. Eng. Chem. Res.* **35** (1996) 1824–1833.
11. Murzin, D. Yu.; Sokolova, N. A.; Kul'kova, N. V.; Temkin, M. I. Kinetics of Liquid-Phase Hydrogenation of Benzene and Toluene on a Nickel Catalyst. *Kinet. Katal.* **30** (1989) 1352–1358.
12. Smeds, S.; Salmi, T.; Murzin, D. Yu. On the Kinetic Coupling and Mechanism of the Aromatic Ring Hydrogenation. *React. Kinet. Catal. Lett.* **63** (1998) 47–51.

13. Cooper, B. H.; Donnis, B. B. L. Aromatic Saturation of Distillates: An Overview. *Appl. Catal. A: Gen.* **137** (1996) 203–223.
14. Stanislaus, A.; Cooper, B. H. Aromatic Hydrogenation Catalysis: A Review. *Catal. Rev. –Sci. Eng.* **36** (1994) 75–123.
15. Nishijima, A.; Kameoka, T.; Sato, T.; Matsubayashi, N.; Nishimura, Y. Catalyst Design and Development for Upgrading Aromatic Hydrocarbons. *Catal. Today* **45** (1998) 261–269.
16. Bergem, H. Sulfur Tolerant Zeolite Supported Platinum Catalysts for Aromatics Hydrogenation. *Ph.D. Thesis*; NTNU, Trondheim, Norway, 1997, 155 p.
17. Korre, S. C.; Klein, M. T.; Quann, R. J. Polynuclear Aromatic Hydrocarbons Hydrogenation. 1. Experimental Reaction Pathways and Kinetics. *Ind. Eng. Chem. Res.* **34** (1995) 101–117.
18. Toppinen, S.; Salmi, T.; Rantakylä T.-K.; Aittamaa, J. Liquid-Phase Hydrogenation Kinetics of Aromatic Hydrocarbon Mixtures. *Ind. Eng. Chem. Res.* **36** (1997) 2101–2109.
19. Horiuchi, J.; Polanyi, M. Exchange Reactions of Hydrogen on Metallic Catalysts. *Trans. Faraday Soc.* **30** (1934) 1164–1172.
20. Augustine, R. L.; Yaghmaie, F.; Van Peppen, J. F. Heterogeneous Catalysis in Organic Chemistry. 2. A Mechanistic Comparison of Noble-Metal Catalysts in Olefin Hydrogenation. *J. Org. Chem.* **49** (1984) 1865–1870.
21. Cortright, R. D.; Levin, P. E.; Dumesic, J. A. Kinetic Studies of Isobutane Dehydrogenation and Isobutene Hydrogenation over Pt/Sn-Based Catalysts. *Ind. Eng. Chem. Res.* **37** (1998) 1717–1723.
22. Cremer, P. S.; Su, X.; Shen, Y. R.; Somorjai, G. A. Ethylene Hydrogenation on Pt(111) Monitored in Situ at High Pressures Using Sum Frequency Generation. *J. Am. Chem. Soc.* **118** (1996) 2942–2949.
23. Cremer, P. S.; Su, X.; Shen, Y. R.; Somorjai, G. A. Hydrogenation and Dehydrogenation of Propylene on Pt(111) Studied by Sum Frequency Generation from UHV to Atmospheric Pressure. *J. Phys. Chem.* **100** (1996) 16302–16309.

24. Mohsin, S. B.; Trenary, M.; Robota, H. J. Identification of Ethylene-Derived Species on Al₂O₃-Supported Rh, Ir, Pd, and Pt Catalysts by Infrared Spectroscopy. *J. Phys. Chem.* **95** (1991) 6657-6661.
25. Cremer, P.; Stanners, C.; Niemantsverdriet, J. W.; Shen, Y. R.; Somorjai, G. The Conversion of di- σ Bonded Ethylene to Ethylidyne on Pt(111) Monitored with Sum Frequency Generation: Evidence for an Ethylidene (or Ethyl) Intermediate. *Surf. Sci.* **328** (1995) 111–118.
26. Mohsin, S. B.; Trenary, M.; Robota, H. J. Infrared Identification of the Low-Temperature Forms of Ethylene Adsorbed on Pt/Al₂O₃. *J. Phys. Chem.* **92** (1988) 5229–5233.
27. Beebe, T. P., Jr.; Albert, M. R.; Yates, J. T., Jr. Infrared Spectroscopic Observation and Characterization of Surface Ethylidyne on Supported Palladium on Alumina. *J. Catal.* **96** (1985) 1–11.
28. Davis, S. M.; Zaera, F.; Gordon, B. E.; Somorjai, G. A. Radiotracer and Thermal Desorption Studies of Dehydrogenation and Atmospheric Hydrogenation of Organic Fragments Obtained from [14C]Ethylene Chemisorbed over Platinum(111) Surfaces. *J. Catal.* **92** (1985) 240–246.
29. Rekoske, J. E.; Cortright, R. D.; Goddard, S. A.; Sharma, S. B.; Dumesic, J. A. Microkinetic Analysis of Diverse Experimental Data for Ethylene Hydrogenation on Platinum. *J. Phys. Chem.* **96** (1992) 1880–1888.
30. Kiperman, S. L. Some Problems of Chemical Kinetics in Heterogeneous Hydrogenation Catalysis. *Stud. Surf. Sci. Catal.* **27** (1986) 1–52.
31. Mints-Eya, V.; Hilaire, L.; Choplin, A.; Touroude, R.; Gault, F.G. The Reaction of Deuterium with Olefins on Nickel Catalysts: Evidence for Adsorbed Vinylic Species. *J. Catal.* **82** (1983) 267–278.
32. Fukushima, T.; Ozaki, A. The Nature of Adsorbed Olefin over Nickel Oxide as Revealed by Competitive Hydrogenation. *J. Catal.* **59** (1979) 465–466.
33. Biloen, P.; Dautzenberg, F. M.; Sachtler, W. M. H. Catalytic Dehydrogenation of Propane to Propene over Platinum and Platinum-Gold Alloys. *J. Catal.* **50** (1977) 77–86.

34. Sachtler, W. M. H.; Van der Plank, P. The Role of Individual Surface Atoms in Chemisorption and Catalysis by Nickel-Copper Alloys. *Surf. Sci.* **18** (1969) 62–79.
35. Sinfelt, J. H.; Carter, J. L.; Yates, D. J. C. Catalytic Hydrogenolysis and Dehydrogenation over Copper-Nickel Alloys. *J. Catal.* **24** (1972) 283–296.
36. Johnson, R.; Pankow, J.; Bender, D.; Price, C.; Zogorski, J. MTBE — To What Extent Will Past Releases Contaminate Community Water Supply Wells? *Environ. Sci. Tech.* **34** (2000) 210A–217A.
37. Squillace, P. J.; Moran, M. J.; Lapham, W. W.; Price, C. V.; Clawges, R. M.; Zogorski, J. S. Volatile Organic Compounds in Untreated Ambient Groundwater of the United States, 1985–1995. *Environ. Sci. Tech.* **33** (1999) 4176–4187.
38. Williams, P. R. D. MTBE in California Drinking Water: An Analysis of Patterns and Trends. *Environ. Forensics* **2** (2001) 75–85.
39. Sloan, H. D.; Birkhoff, R.; Gilbert, M. F.; Nurminen, M.; Pyhälähti, A. Isooctane Production from C₄'s as an Alternative to MTBE. Presented at the NPRA 2000 Annual Meeting, San Antonio, TX, Mar 26–28, 2000; Paper AM-00-34.
40. Trotta, R.; Marchionna, M.; Amoretto, F. An Iso-Octane Technology to Produce Alkylate Streams. *Today's Refinery* **10** (1999) 21–24.
41. Rautanen, P. A. Liquid-Phase Hydrogenation of Aromatic Compounds on Nickel Catalyst. *Doctoral Thesis*; Helsinki University of Technology, Espoo, Finland, 2002, pp. 11–13.
42. Backman, L. B.; Rautiainen, A.; Lindblad, M.; Jylhä, O.; Krause, A. O. I. Characterisation of Co/SiO₂ Catalysts Prepared from Co(acac)₃ by Gas Phase Deposition. *Appl. Catal. A: Gen.* **208** (2001) 223–234.
43. Zowtiak, J. M.; Bartholomew, C. H. The Kinetics of Hydrogen Adsorption on and Desorption from Cobalt and the Effects of Support Thereon. *J. Catal.* **83** (1983) 107–120.
44. Reuel, R. C.; Bartholomew, C. H. The Stoichiometries of Hydrogen and Carbon Monoxide Adsorptions on Cobalt: Effects of Support and Preparation. *J. Catal.* **85** (1984) 63–77.

45. Satterfield, C. *Mass Transfer in Heterogeneous Catalysis*. MIT Press, Cambridge MA, 1970, pp. 38–39.
46. Moysan, J. M.; Huron, M. J.; Paradowski, H.; Vidal, J. Prediction of the Solubility of Hydrogen in Hydrocarbon Solvents through Cubic Equations of State. *Chem. Eng. Sci.* **38** (1983) 1085–1092.
47. Park, J.; Robinson, R. L., Jr.; Gasem, K. A. M. Solubilities of Hydrogen in Heavy Normal Paraffins at Temperatures from 323.2 to 423.2 K and Pressures to 17.4 MPa. *J. Chem. Eng. Data* **40** (1995) 241–244.
48. Park, J.; Robinson, R. L., Jr.; Gasem, K. A. M. Solubilities of Hydrogen in Aromatic Hydrocarbons from 323 to 433 K and Pressures to 21.7 MPa. *J. Chem. Eng. Data* **41** (1996) 70–73.
49. Reid, R. C.; Prausnitz, J. M.; Poling, B. E. *The Properties of Gases and Liquids*. 4th Ed., McGraw-Hill, Boston MA, 1987, p. 598.
50. Harriott, P. Thermal Conductivity of Catalyst Pellets and Other Porous Particles. Part I: Review of Models and Published Results. *Chem. Eng. J.* **10** (1975) 65–71.
51. Sharma, C. S.; Harriott, P.; Hughes, R. Thermal Conductivity of Catalyst Pellets and Other Porous Particles. Part II: Experimental Measurements. *Chem. Eng. J.* **10** (1975) 73–80.
52. Froment, G. F.; Bischoff, K. B. *Chemical Reactor Analysis and Design*. 2nd Ed., John Wiley & Sons, Singapore, 1990, 664 p.
53. Aittamaa, J. R.; Keskinen, K. I. *Flowbat—User's Instruction Manual*. Laboratory of Chemical Engineering, Helsinki University of Technology, Espoo, Finland, 2000.
54. Villadsen, J.; Michelsen, M. *Solution of Differential Equation Models by Polynomial Approximation*. Prentice-Hall, New Jersey, 1978, p. 317.
55. Brown, P. N.; Byrne, G. D.; Hindmarsh, A. C. VODE: A Variable-Coefficient ODE Solver. *SIAM J. Sci. Stat. Comp.* **10** (1989) 1038–1051.
56. Weitkamp, A. W. Stereochemistry and Mechanism of Hydrogenation of Naphthalenes on Transition Metal Catalysts and Conformational Analysis of the Products, *Adv. Catal.* **18** (1968) 1–110.

57. Huang, T.-C.; Kang, B.-C. Kinetic Study of Naphthalene Hydrogenation over Pt/Al₂O₃ Catalyst. *Ind. Eng. Chem. Res.* **34** (1995) 1140–1148.
58. Smith, G. V.; Burwell, R. L., Jr. Reactions between Deuterium and Olefins in the Liquid Phase on Platinum Oxide Catalysts. *J. Am. Chem. Soc.* **84** (1962) 925–934.
59. Shiraishi, Y.; Taki, Y.; Hirai, T.; Komasaawa, I. A Novel Desulfurization Process for Fuel Oils Based on the Formation and Subsequent Precipitation of S-Alkylsulfonium Salts. 1. Light Oil Feedstocks. *Ind. Eng. Chem. Res.* **40** (2001) 1213–1224.
60. Toppinen, S.; Rantakylä, T.-K.; Salmi, T.; Aittamaa, J. The Liquid Phase Hydrogenation of Benzene and Substituted Alkylbenzenes over a Nickel Catalyst in a Semi-Batch Reactor. *Catal. Today* **38** (1997) 23–30.
61. Toppinen, S.; Rantakylä, T.-K.; Salmi, T.; Aittamaa, J. Kinetics of the Liquid Phase Hydrogenation of Di- and Trisubstituted Alkylbenzenes over a Nickel Catalyst. *Ind. Eng. Chem. Res.* **35** (1996) 4424–4433.
62. Tjandra, S.; Zaera, F. A Surface Science Study of the Hydrogenation and Dehydrogenation Steps in the Interconversion of C₆ Cyclic Hydrocarbons on Ni(100). *J. Catal.* **164** (1996) 82–93.
63. Lehwald, S.; Ibach, H.; Demuth, J. E. Vibration Spectroscopy of Benzene Adsorbed on Pt(111) and Ni(111). *Surf. Sci.* **78** (1978) 577–590.
64. Friend, C. M.; Muetterties, E. L. Coordination Chemistry of Metal Surfaces. 3. Benzene and Toluene Interactions with Nickel Surfaces. *J. Am. Chem. Soc.* **103** (1981) 773–779.
65. Temkin, M. I. The Kinetics of Some Industrial Heterogeneous Catalytic Reactions. *Adv. Catal.* **28** (1979) 173–281.
66. Toppinen, S.; Rantakylä, T.-K.; Salmi, T.; Aittamaa, J. Kinetics of the Liquid-Phase Hydrogenation of Benzene and Some Monosubstituted Alkylbenzenes over a Nickel Catalyst. *Ind. Eng. Chem. Res.* **35** (1996) 1824–1833.
67. Jonker, G. H.; Veldsink, J.-W.; Beenackers, A. A. C. M. Intrinsic Kinetics of 9-Monoenic Fatty Acid Methyl Ester Hydrogenation over Nickel-Based Catalysts. *Ind. Eng. Chem. Res.* **36** (1997) 1567–1579.

68. Kut, O. M.; Dätwyler, U. R.; Gut, G. Stereoselective Hydrogenation of 2-*tert*-Butylphenol to *cis*-2-*tert*-Butylcyclohexanol. 2. Kinetics of the Liquid-Phase Hydrogenation of 2-*tert*-Butylphenol over Nickel, Cobalt, and Noble Metal Catalysts. *Ind. Eng. Chem. Res.* **27** (1988) 219–225.
69. Rautanen, P. A.; Aittamaa, J. R.; Krause, A. O. I. Solvent Effect in Liquid-Phase Hydrogenation of Toluene. *Ind. Eng. Chem. Res.* **39** (2000) 4032–4039.
70. Boitiaux, J. P.; Cosyns, J.; Robert, E. Liquid Phase Hydrogenation of Unsaturated Hydrocarbons on Palladium, Platinum, and Rhodium Catalysts. Part I: Kinetic Study of 1-Butene, 1,3-Butadiene and 1-Butyne Hydrogenation on Platinum. *Appl. Catal.* **32** (1987) 145–168.
71. Pecque, M.; Maurel, R. Hydrogénation Catalytique IV. Hydrogénation en Phase Liquide de Couples d'Oléfines Isomères de Position. *Bull. Soc. Chim. Fr.* **6** (1969) 1882–1887.
72. Bartholomew, C. H. Mechanisms of Catalyst Deactivation. *Appl. Catal. A: Gen.* **212** (2001) 17–60.
73. Taya, K.; Morimoto, S.; Abe, C.; Nomura, K.; Nomura, O.; Tanaka, K. Substituent Effects in Heterogeneous Catalysis. VI. Competitive Hydrogenation of Methylene cyclohexane and 2-Methylmethylene cyclohexane over Platinum Group Metals. *Bull. Chem. Soc. Japan* **53** (1980) 1034–1038.
74. Kieboom, A. P. G.; Van Bekkum, H. Electronic Substituent Effects on the Adsorption and Hydrogenation of the Olefinic Bond on Palladium. *J. Catal.* **25** (1972) 342–349.
75. Ramachandran, P. A.; Chaudhari, R. V. *Three-Phase Catalytic Reactors*. Gordon and Breach Science Publishers, London, 1983, p. 194.
76. Campelo, J. M.; Garcia, A.; Luna, D.; Marinas, J. M. Liquid Phase Catalytic Hydrogenation of 1-Hexene on AlPO₄-Supported Nickel Catalysts. *Appl. Catal.* **3** (1982) 315–325.
77. Boutonnet, M.; Andersson, C.; Larsson, R. Liquid Phase Hydrogenation of 1-Hexene and 2-Hexene with 30-Å Platinum Particles on Alumina Support. *Acta Chem. Scand. A: Phys. Inorg. Chem.* **34** (1980) 639–644.

78. Gardin, D. E.; Su, X.; Cremer, P. S.; Somorjai, G. A. Liquid-Phase Hydrogenation of Cyclohexene over Pt Foil Catalysts. *J. Catal.* **158** (1996) 193–198.
79. Wilhite, B. A.; McCready, M. J.; Varma, A. Kinetics of Phenylacetylene Hydrogenation over Pt/ γ -Al₂O₃ Catalyst. *Ind. Eng. Chem. Res.* **41** (2002) 3345–3350.
80. Asinger, F. *Mono-Olefins: Chemistry and Technology*. Pergamon Press, Oxford, 1968, p. 455.
81. Di Gerolamo, M.; Catani, R.; Marchionna, M. Process and Catalysts for the Hydrogenation of Branched Olefins Derived from the Dimerization of Isobutene in the Manufacture of High-Octane Fuels. *U.S. Pat. Appl. Publ. 20030078462* (2003), p. 5.